Author manuscript

Med Image Anal. Author manuscript; available in PMC 2018 April 01.

Published in final edited form as:

Med Image Anal. 2017 April ; 37: 129–145. doi:10.1016/j.media.2017.02.002.

Involuntary Eye Motion Correction in Retinal Optical Coherence Tomography: Hardware or Software Solution?

Ahmadreza Baghaie[1,*], **Zeyun Yu**[2], and **Roshan M. D'Souza**[3]

[1]Department of Electrical Engineering, University of Wisconsin-Milwaukee, WI, USA

[2]Department of Computer Science, University of Wisconsin-Milwaukee, WI, USA

[3]Department of Mechanical Engineering, University of Wisconsin-Milwaukee, WI, USA

Abstract

In this paper, we review state-of-the-art techniques to correct eye motion artifacts in Optical Coherence Tomography (OCT) imaging. The methods for eye motion artifact reduction can be categorized into two major classes: 1) hardware-based techniques and 2) software-based techniques. In the first class, additional hardware is mounted onto the OCT scanner to gather information about the eye motion patterns during OCT data acquisition. This information is later processed and applied to the OCT data for creating an *anatomically correct* representation of the retina, either in an offline or online manner. In software based techniques, the motion patterns are approximated either by comparing the acquired data to a reference image, or by considering some prior assumptions about the nature of the eye motion. Careful investigations done on the most common methods in the field provides invaluable insight regarding future directions of the research in this area. The challenge in hardware-based techniques lies in the implementation aspects of particular devices. However, the results of these techniques are superior to those obtained from software-based techniques because they are capable of capturing secondary data related to eye motion during OCT acquisition. Software-based techniques on the other hand, achieve moderate success and their performance is highly dependent on the quality of the OCT data in terms of the amount of motion artifacts contained in them. However, they are still relevant to the field since they are the sole class of techniques with the ability to be applied to legacy data acquired using systems that do not have extra hardware to track eye motion.

Graphical Abstract

Corresponding author: abaghaie@uwm.edu.

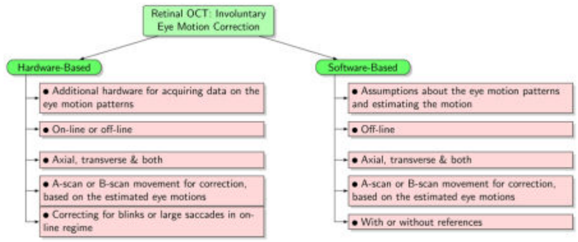

Keywords

Retina; Optical Coherence Tomography (OCT); Motion Artifact Correction

1. Introduction

Optical Coherence Tomography (OCT) is a powerful non-invasive imaging system for acquiring 3D volumetric images of tissues (Huang et al. (1991), Tomlins and Wang (2005)). OCT as an optical imaging modality, aims to provide cross-sectional images of tissues by measuring the magnitude of back-scattered/back-reflected light as well as the echo time delay (Drexler and Fujimoto (2008), Wojtkowski (2010)). The concept resembles that of ultrasound, however, due to high speed of light, direct measurement of the optical echo is impossible. This calls for indirect procedures for measuring the time-of-flight and intensity of the back-scattered light which is done by taking advantage of interferometric techniques using ultra-short light pulses or partially coherent light (Fercher (1996), Fercher et al. (2003)). Throughout the past two decades, new developments in the OCT imaging systems have improved the acquisition time and also the quality of the acquired images. Nowadays taking μm-resolution volumetric images of the tissues is very common especially in ophthalmology.

Generally speaking, there are three main tasks in retinal OCT image processing (Baghaie et al. (2015b)): noise reduction, segmentation, and image registration. The process of OCT image acquisition results in the formation of irregular granular patterns called speckle. This is not only limited to OCT imaging. In fact, speckle is a fundamental property of signals and images acquired by narrow-band detection systems, including Synthetic Aperture Radar (SAR) and ultrasound. In OCT, not only the optical properties of the system, but also the motion of the subject to be imaged, size and temporal coherence of the light source, multiple scattering, phase deviation of the beam and aperture of the detector can affect the speckle pattern. Two types of speckle are present in OCT images: a) signal-carrying speckle which originates from the sample volume in the focal zone; and b) signal-degrading speckle, also known as speckle noise, which is created by multiply-scattered out-of-focus light (Schmitt et al. (1999)). OCT noise reduction techniques can be divided into two major classes: 1) methods of noise reduction during the acquisition time and 2) post-processing techniques. In the first class, also known as compounding techniques, multiple uncorrelated recordings are averaged. Techniques in this class include spatial compounding (Avanaki et al. (2013)), angular compounding (Schmitt (1997)), polarization compounding (Kobayashi et al. (1991)) and frequency compounding (Pircher et al. (2003)). As for post-processing techniques, anisotropic diffusion based methods (Salinas and Fernández (2007), Puvanathasan and Bizheva (2009)), multiscale/multiresolution geometric representation based techniques (Pizurica et al. (2008), Adler et al. (2004), Jian et al. (2009, 2010), Guo et al. (2013), Xu et al. (2013), Gupta et al. (2014)) and compressive sensing and sparse representation based approaches (Fang et al. (2012, 2013)) are good examples.

Delineating micro-structures in the image is of particular importance in OCT image processing for ophthalmology (DeBuc (2011), Kafieh et al. (2013b)) and therefore image segmentation plays a significant role in OCT data analysis, especially retinal layer segmentation. Active contour based techniques (Fernández et al. (2004), Mishra et al. (2009), Yazdanpanah et al. (2011)) and graph-based techniques (Kafieh et al. (2013a), Garvin et al. (2008), Chiu et al. (2010, 2012), Srinivasan et al. (2014)) are very good examples of such approaches.

There are several different applications for using image registration approaches in OCT image analysis, such as noise reduction (Jørgensen et al. (2007), Alonso-Caneiro et al. (2011), Baghaie et al. (2016, 2015a)), multi-modal retinal image registration (Li et al. (2011a), Golabbakhsh and Rabbani (2013)), image mosaicing (Li et al. (2011b), Hendargo et al. (2013), Lurie et al. (2014)), and motion correction (Pircher et al. (2007), Ricco et al. (2009), Xu et al. (2012), Kraus et al. (2012, 2014)).

In this paper, we focus on the problem of artifacts in 3D volumetric OCT scans resulting from involuntary eye motions during acquisition. We provide detailed analysis of various techniques in the field and highlight the relative advantages and disadvantages. Our review will not only cover general OCT devices but will also include other related imaging modalities such as adaptive optics (AO) OCT, phase stabilized (PS) OCT, and transverse scanning (TS) OCT. In section 2, we will discuss in detail the problem of involuntary eye motion artifacts. Section 3 contains comprehensive and detailed introduction to the state-of-the-art in the field and discusses both hardware-based and software-based solutions. Sections 4 summarizes the reviewed approaches and provides additional discussions regarding their limitations. Sections 5 concludes the paper.

2. Involuntary Eye Motion Artifacts in OCT Imaging

The visual system in governed by neural adaptation in which constant illumination causes weak neural responses while sudden changes in illumination across space and time will result in strong responses. In such a system, unchanging features fade away from the view and eye movements during fixation become a necessity to overcome the loss of vision, even at the price of having lower visual acuity (Riggs et al. (1953), Nachmias (1959), Martinez-Conde et al. (2004)). Eye motions during fixation are divided into three main types: tremor, drifts and microsaccades (Barlow (1952), Yarbus (1967), Carpenter (1988)). Tremor is a not-periodic wavelike motion with a frequency of approximately 90 Hz with very low amplitudes. Drifts occur at the same time as tremor and are slow motions which appear during the intervals between microsaccades. They are proven to have a significant role in maintaining fixation in the absence of microsaccades. During drifts, the image of the fixated object can move across a dozen photoreceptors in the retina. Microsaccades on the other hand, occur during voluntary fixation and are small, fast, jerk-like eye movements. The object's image on the retina can move from several dozens to several hundred photoreceptors during microsaccades. Microsaccades's duration is about 25 milliseconds. They are thought to be useful in counteracting receptor adaptation and also correcting fixation errors (Martinez-Conde et al. (2004)).

There are other sources of eye motion which can have big impacts on the quality of the acquired OCT data. For example, head movements during the acquisition time can cause the subject's retina to move completely out of focus of the imaging beam. Movements caused by heartbeats and the respiration system can also cause severe axial motion artifacts (de Kinkelder et al. (2011)). This can be seen mostly by observing orthogonal cross-sections of the acquired OCT volume where the true curvature of the retina is completely compromised. This type of artifact is even visible in the volume scans acquired by ultrahigh speed OCT devices.

The methods for eye motion correction can be categorized into two major classes: 1) hardware-based techniques; 2) software-based techniques. Hardware-based techniques use additional hardware mounted onto the OCT system to acquire information related to the eye motion patterns during the OCT data acquisition. The additional information (apex of the cornea or 2D view of the scan site or etc) serves as means for approximating the eye motion and is used for correcting the OCT volume, either by moving A-scans or B-scans. Motion correction can be done in an online manner which means that processing of the additional data is happening at the same time as data acquisition, or can be offline. Online correction of eye motion provides us with the possibility of detecting the artifacts that can cause severe loss of data, like blinks or large saccades. In such cases, a signal can be sent to the OCT device indicating the need for re-scanning of the affected regions. This is not possible in offline hardware-based techniques. In software-based techniques, no additional data is acquired during the acquisition time, therefore, there is no explicit data related to eye motion. Eye motion has to be computed from the OCT data itself.

At any given time, eye motion is a combination of translations and rotations in three dimensions. In the OCT volume data sets, one has only the 1D and 2D projections of these 3D motions. In hardware-based techniques the objective is to solve the **forward** problem by acquiring additional information about the eye motion patterns during OCT acquisition. On the other hand, software-based techniques try to solve the highly nonlinear and ill-posed **inverse** problem by estimating the eye motion patterns from the acquired OCT data.

Even though the subject of the imaging is asked to fixate, involuntary eye motions still happen, with different amplitudes in different directions at the time of acquisition. Figure 1 shows a sample OCT volume scan with the corresponding A-scan axis (AA), fast-scanning axis (FA) and slow-scanning axis (SA). Axial motion artifacts can be observed by looking at the view orthogonal to the plane created by the A-scan and slow-scanning axes. On the other hand, transverse motions can be observed by looking at the *en face* view of the OCT data, the projection along the axial direction. They are most representative in regions with prominent features like blood vessels. Micro-saccades represent themselves as breaks along the fast scanning axis while drifts are responsible for shrunk and expanded regions in the

OCT data. These introduce a big challenge for software-based motion correction techniques since each one of these motions require different models for representation. Eye motions in the direction of slow scanning axis can cause gaps (if the motion happens in opposite direction) or multiple copies of some portion of the data (if the motion happens in the same direction). This is mainly problematic because there is no way to have an accurate measurement of such motions since there is no ground truth for the 3D *in vivo* human retina. Of course no hardware-based technique needs to worry about this because if one has access to the eye motion patterns during the acquisition time, one can always apply the inverse motion to the OCT data. But this is not the case for software-based techniques. Because of this, all of the software-based techniques need some prior assumptions about the eye motion which as one can imagine, usually mean having limited settings for data acquisition and limited amount of motion artifacts. Even then, it is not possible to reconstruct a completely anatomically-accurate 3D volume of the retina and at most, an approximation is given which can be far from the truth due to severe non-linearity and ill-posedness of the problem. A rigorous quantitative analysis of the extents of involuntary eye motion artifacts should take into account the various intertwined parameters involved. OCT imaging devices and their corresponding limitations and configurations are the first that come to mind. Not only the scanning speed of the devices in terms of A-scans/s but also the number of A-scans (or B-scans) that make up a B-scan (or volume) as well as the scan area can have a large impact on the amount and severity of eye motions in the acquired data. The subjects to be imaged and whether they suffer from retinal diseases or not also plays an important role. The type of the data that is required for the subsequent processing may dictate specific corrections. For example, if only motion artifact reduction/correction for an *en face* or a projection view is required, axial motion artifacts may be ignored. However, it should be noted that while this is a common practice in the literature, residual artifacts due to involuntary axial motions still remain present in the data. Another limitation is in regards to the lack of complete/accurate reference data in order to be able to have a more quantitative assessment of the approaches. While various imaging techniques are available to produce fast motion artifact-free *en face* images of the retina, however, when dealing with 3D volume scans no such reference is available. This mainly results in lack of proper comparisons between different techniques proposed for correcting motion artifacts, as can be seen in the literature. All the aforementioned factors make the assessment of various techniques for involuntary eye motion correction of retinal optical coherence tomography data, especially software-based approaches, to not be a trivial task. The first step can be to carefully design procedures for generating simulated datasets with known ground truth as means for assessing the performance of various techniques.

Several commercially available OCT imaging devises have already included additional hardware for eye motion correction. Spectralis HRA-OCT (Heidelberg-Engineering (Accessed: 11-10-2016)) uses a real time eye motion tracking system to track eye movements and guide OCT to the proper location for repeating the B-scans if there was eye movement during scanning. The tracking system is an effective solution for transverse movements, while axial correction still requires a software correction. In Cirrus HD-OCT (Carl-Zeiss-Meditec (Accessed: 11-10-2016)) in addition to the 3-D raster scans, the device acquires two diagonal B-scans that are mainly used for axial motion correction. In the

RTVue system (Optovue-Inc. (Accessed: 11-10-2016)) the motion is measured at 30 Hz from an infrared full-field fundus camera. The PSI system (Physical-Sciences-Inc. (Accessed: 11-10-2016)) uses a non-imaging method where a dithering beam is used to lock on reflectance changes from single retinal features within the optic nerve head (ONH) or on blood vessels. Canon OCT-HS100 (Canon-Europa-N.V (Accessed: 11-10-2016)), as another example, uses both automatic anterior eye alignment and fundus tracking for better compensation of involuntary eye motions during image acquisition. It is expected that all of OCT devices will have hardware-based eye motion correction in the next few years.

The following section contains detailed elaboration on some of the very well-known hardware/software based techniques used for correcting eye motion in OCT data. The study is not limited to only general OCT and also includes other variations of OCT imaging like AO-OCT, TS-OCT and OCT angiography. The main focus here was on the eye motion correction aspects of the proposed techniques and minimal and *get-to-the-point* information is given regarding the design of the imaging devices. So the avid reader is encouraged to refer to the corresponding resources for more details on the design and implementation of the devices.

A detail that should be clarified before moving forward is that the categorization of the techniques into two major classes, namely hardware-based and software-based, should not cause confusions in regards to the software used in hardware-based techniques. To be more precise, analyzing the additional data acquired by hardware-based techniques requires custom software and in a sense, hardware-based techniques can be considered as a *hybrid*. However, since in the majority of the techniques introduced here the needed software is not the main focus of the paper (this becomes more obvious when knowing almost all of the utilized software are variations of cross-correlation-based image registration technique), we have not based our classification on this fact. Instead, the classification is based on the fact that whether an approach acquires additional information about the eye motion patterns during OCT acquisition by using additional hardware in the system or solely relies on the final OCT data. Table 1 gives a brief overview of the methods for involuntary eye motion correction in OCT data. More details are given in the following sections.

3. Methods

3.1. Hardware-Based Approaches

Hardware-based involuntary eye motion reduction techniques involve mounting additional hardware on the OCT machines for capturing eye motion (axial and/or transverse) and then applying the inverse motion to A-scans/B-scans, either in an online manner or as a post-processing step. In online techniques, being able to detect and correct the motion allows for better compensation of the severe eye motions including large saccades and also blinks. In such techniques, messages can be passed between the tracking device and the OCT machine indicating the need for re-acquiring the portion of the data that was affected. Overall, hardware-based techniques can provide better results in comparison to software-based techniques in terms of accuracy and reliability. Using these techniques, it is possible to reconstruct *anatomically correct* volume scans of retina which can be very helpful in tracking the morphology of the retina, progress of the diseases and the effect of medications in longitudinal studies. Such techniques have been already implemented in some commercial devices as mentioned in the previous section and in a few years, will be commonplace in all clinical settings. Here a literature review of a few of very prominent techniques for hardware-based eye motion correction in OCT imaging is provided.

Ferguson et al. (2004) tested an experimental tracking optical coherence tomography (OCT) system in a clinical setting. The device uses a secondary sensing beam and steering mirrors to compensate for eye motion with a closed-loop bandwidth of 1 kHz and tracking accuracy, to within less than the OCT beam diameter. The retinal tracking prototype works based on projecting a low-power beam ($<25\ \mu W$ at 860 nm) onto retinal features with contrast relative to their neighboring areas (blood vessel junctions, the lamina cribrosa, retinal lesions, drusen, scars or irregular pigmentation, for example). The tracking beam is circularly wavered at 8 kHz with an amplitude of 150 μm on the retina with a pair of resonant scanners. This beam is detected with a confocal reflectometer and processed with a dual-phase lock-in amplifier to produce directional error signals. The interference from corneal reflections in the confocal reflectometer are reduced using a split aperture. The tracking beam is directed onto the retina by a galvanometer-driven tracking mirror pair and real-time digital signal processing is being employed for extracting the position and orientation information from optical error signals to make precise closed-loop beam-steering corrections. Since the OCT scans are also reflected from the tracking mirrors, the OCT beam automatically follows any movement of the retina with the same speed and precision as the tracking beam.

In the work of Pircher et al. (2007), use of simultaneous scanning laser ophthalmoscopy (SLO) and OCT imaging is investigated for axial motion correction in imaging of the human retina. Using an additional spectral domain partial coherence interferometer (SD-PCI) integrated into a transverse scanning (or *en-face*) optical coherence tomography (TS-OCT) system, they were able to measure the position of cornea which is later used for correcting the axial motion. Their setup consists of two parts: A high speed TS-OCT system operating at 840nm (Pircher et al. (2006a)), and a spectral domain partial coherence interferometer (SD-PCI) operating at 1310nm. In the former part a Mach Zehnder interferometer is used with a light source of 50nm bandwidth that results in a depth resolution of approximately $6\mu m$ in air. The later fiber based SD-PCI is operated by a light source of 55nm band with which results in a depth resolution of approximately $14\mu m$. The position of the cornea is determined by using a peak detection algorithm applied to the resulting coherence function from SD-PCI. The measured position is utilized to drive a voice coil translation stage in the reference arm of the TS-OCT. It should be mentioned that the two systems were performing independently and the update time of approximately $5ms$ was achieved. The depth correction system is operating with a proportional control algorithm. Using this system they were able to correct the axial motion artifacts significantly.

In their later work, Pircher et al. (2010) improved the previous system to be able to correct the transverse eye motion artifacts on a cellular level. Unlike the previous system, here, the prototype consists of three major components: 1) a main Mach Zehnder interferometer, 2) an auxiliary spectral domain low coherence interferometer (SD-LCI) operating at 1300nm and 3) a rapid scanning optical delay line (RSOD) located in the reference arm of the main interferometer. The axial motion correction is done by measuring the position of the apex of the cornea using the SD-LCI which is later used to drive the RSOD. The main interferometer is designed to record SLO and OCT images simultaneously, in vivo and with a cellular resolution. Each scan takes up to 3 seconds and contains 120 frames in a 1° × 1° area, with 700μm or 200μm in depth. The SLO images are 2D views of the area while OCT scan contains B-scans depicting cross-sections of the depth. For correcting the transverse eye motion artifacts, at first, all of the frames in the SLO image sequence are registered to a manually selected reference frame from the sequence and averaged. The result of the first step is used as the reference for the second step which again involves registering SLO frames. This way, they were able to reduce the effects of small distortions in the previous reference frame. The result of the second step is represented as a translation matrix which is further used for correcting OCT images. It should be mentioned that the OCT and SLO images have pixel to pixel correspondence. Combining the axial and transverse motion corrected volumes allows for additional minimization of the errors (differing light coupling ratio into cone photoreceptors and residual depth tracking errors, for example).

In the same year, Tao et al. (2010) combined a spectrally encoded confocal scanning laser ophthalmoscope (SECSLO) with an ophthalmic SD-OCT system for being able to capture video-rate SLO images alternately with high-resolution SD-OCT B-scans. Combining these two techniques, they were able to improve image aiming, guidance and registration as well as eye motion compensation. The illumination source, detections systems and scanning optics are very similar between these two modalities which provide us with the possibility of sharing them between the two. This sharing allows for inherent co-registration of the SLO and OCT data. In the proposed system, the galvanometers are driven such that 200 interlaced frames are captured over the SD-OCT volume, where 100 of these frame are 2D SEC-SLO fundus images and the rest are depth-resolved SD-OCT B-scans. The imaging procedure takes up to 10 seconds, covering an area of $5 \times 3mm^2$. As a post-processing step, the SLO frames are co-registered and the transformation matrices are used for compensating the gross motion of the SD-OCT B-scans. Using this technique, they were able to correct the transverse eye motion artifacts, while axial motion is still present in the volume data. Of course, the *en face* view of the corrected OCT volume can be considered as an anatomically correct representation of the retina. Figure 2 shows an example of this technique for involuntary transverse motion correction.

Introduction of adaptive optics into OCT systems provides a means for acquiring cellular resolution 3D volume scans. In the work of Capps et al. (2011) simultaneous acquiring of adaptive optics-scanning laser ophthalmoscope (AO-SLO) images with AO-OCT volume data is presented as a solution for eye motion correction. The axial motion correction is done by translating the B-scans parallel to the scanning beam for maximizing the cross-correlation. As for transverse motion correction, at first, each AO-SLO frame is divided into seven overlapping horizontal regions (centered at 1/8, 2/8, 3/8,…,7/8 locations of the frame). This is followed by registering each region to the preceding SLO frame which results in a translation vector. Since each SLO frame corresponds to an OCT B-scan, the translation vectors can be applied to the A-scans at 1/8, 2/8, 3/8,…,7/8 locations of each B-scan. A cubic spline interpolation is employed for computing the translation vectors for the rest of the A-scans in each B-scan. Finally, the deformed OCT volume is re-sampled to a regular grid.

In 2012, Vienola et al. (2012) introduced a new tracking OCT system in which a phase-stabilized optical frequency domain imaging (OFDI) system and an eye tracking scanning laser ophthalmoscope (TSLO) are combined. The system is shown to be useful for correcting eye drifts and micro saccades. They also included a routine for correction of blinks and large saccades by triggering a signal to guide the OCT system to re-scan the corrupted B-scans. The OFDI system (Braaf et al. (2011)) uses a 100 kHz swept-source (Axsun Technologies, USA) with a center wavelength of 1050 *nm* and an axial resolution of 4.8 μm (6.5 μm in air). An externally built Mach-Zehnder interferometer is used for calibration and phase-stabilization by aligning A-lines to the same wave numbers (k-space) in post-processing. The TSLO (Sheehy et al. (2012)) uses a super luminescent diode (SLD-371, Superlum, Russia) with a center wavelength of 840 nm as the light source and images the eye with 512×512 pixels frames acquired at 30 Hz over a field size of 4 degrees. A 16 kHz resonant scanner (Electro-Optical Products Corporation) is used for fast-axis (horizontal) scanning and slow-axis (vertical) scanning is performed by a galvo-scanner at 30 Hz (Cambridge Technologies). Real-time implementation was possible by using GPU (GeForce GTX 560) and a Field-Programmable Gate Array (FPGA) board (Virtex 5, Xilinx) for TSLO image acquisition and processing. For estimating the eye motion from TSLO frames, at first, a reference frame is chosen. Then, each consecutive frame is divided into 32 overlapping strips, each of the size 32×512 pixels which provides a motion reporting rate of 960Hz, several times higher than the actual TSLO scan rate. Each of these strips are then registered to the reference frame using cross-correlation as the metric and the computed horizontal and vertical displacements are reversed and applied to the OCT data. As for correcting blinks, large saccades, vertical motions, large drifts and misalignment of the pupil which cause sub threshold correlation between the current frame and the reference frame, an invalid signal is sent to the OCT system indicating the need for re-scanning the earlier B-scans. Figure 3 shows several examples of the data acquired with and without tracking presented in this paper.

Detecting blood-flow in retinal scans can be done by computing the phase changes in between A-scans that are obtained from the same location. This observation led to design of phase-resolved OCT angiography devices which provide a non-invasive approach for blood flow detection. In such systems, unlike the dye based techniques such as fluorescein angiography (FA) (Novotny and Alvis (1961)) and indocyanine green angiography (ICGA) (Yannuzzi et al. (1992)), no dye is injected into the blood-stream. But as one can imagine, having involuntary eye motions makes the process of blood-flow detection unreliable. To address this, Braaf et al. (2013) combined inter-B-scan phase-resolved OCT angiography with real-time eye tracking. The idea here is the same as the one described before by Vienola et al. (2012). A tracking scanning laser ophthalmoscope (TSLO) at 840 nm for providing eye tracking functionality is combined with a phase-stabilized optical frequency domain imaging (OFDI) system at 1040 nm. Considering a TSLO frame as the reference selected by the user, consecutive frames are divided into 32 overlapping strips of 32 pixels height, and then registered to the reference frame. The resulted transformations are reversed and then converted to voltage signals and applied to the waveforms that drive the OFDI galvanometer scanners to correct for transverse retinal motion. As for correcting for blinks and large saccades, a validity signal is created indicating the need for re-scanning the corrupted B-scans. To further reduce the effects of distortions in the TSLO reference frame, the motion correction signals are filtered with a 10Hz cut-off frequency which showed minimal effect on the overall system performance. This is because the eye motion amplitude at frequencies above 10Hz is usually less than 2.5 μm (Sheehy et al. (2012)). To create blood-flow images, two B-scans are acquired at the same location. This is followed by two steps of axial motion correction as described in (Braaf et al. (2012)): first being correcting for large displacements by maximizing cross-correlation in the axial directions between the compared B-scans. Second involves correcting for the residual axial displacements by using histogram-based normalization similar as described by Makita et al. (2006). Finally, by subtraction of the phase information for each set of B-scans, the inter-B-scan phase-differences are calculated. An example of the method presented in this work can be seen in Figure 4.

LaRocca et al. (2013b) combined SLO and OCT imaging systems into a handheld device in 2013. As for sources of SLO and OCT scanners, they used superluminescent diodes (SLDs) operating at 770 $\pm$ 8 nm (Inphenix, Livermore, CA) and 840 $\pm$ 35 nm (Superlum, Moscow, Russia), respectively (LaRocca et al. (2013a)). As before, 2D SLO images are used for eye motion approximation. It should be mentioned that this procedure is done offline unlike some of the previously described techniques. To make the process of registration more robust, at first, SLO images are pre-processed using multi-scale coupled Laplacian of Gaussian (LoG) and Gabor filters (Estrada et al. (2011)). Using these filters, one is able to enhance the contrast of blood vessels in the fundus images and therefore the reliability of the following registrations will increase. Then, after choosing a reference frame from the SLO sequence, the rest of the frames were divided into 15 horizontal strips and then registered to the reference frame (using cross-correlation as metric) in order to compute the horizontal/ vertical displacements for each strip. This coarse approximation is later spline interpolated to find the displacement needed for every line of SLO frames. The final estimation is later used for correcting the transverse eye motion artifacts in the simultaneously acquired OCT volume. The gaps introduced by eye motion are filled using interpolation. An example of combining two SLO-based motion corrected orthogonal OCT volume scans using this technique can be seen in Figure 5.

Zawadzki et al. (2014) use a combination of AO-SLO and AO-OCT for correcting the transverse eye motion artifacts. For OCT they used a 836 nm light with a bandwidth of 112 nm and for SLO, a 683.4 nm light with a bandwidth of 8.2 nm. The SLO and OCT beams share the same path for most of the instrument's sample arm and the SLO frames and OCT B-scans are captured simultaneously. It should be mentioned that both SLO and OCT devices scan the same lateral area of the retina. Because both of the subsystems share the vertical scanning mirror, every pass by the vertical mirror captures both an AO-SLO frame and an AO-OCT B-scan. Therefore any change due to involuntary eye motion is reflected in both the AO-OCT B-scan and the AO-SLO frame (C-scan). Unlike some of the previously mentioned methods, here the reference frame is created by selecting and registering several frames from the AO-SLO frame sequence. Then, each of AO-SLO frames are divided into horizontal strips and registered to the composite reference frame. This is followed by applying the resulting translation matrices to the AO-OCT A-scans. The axial motion

Author Manuscript

Author Manuscript

Author Manuscript

artifacts are compensated by maximizing the cross-correlation between adjacent B-scans. Finally, resampling of the scattered A-scans to a regular 3D grid is done by use of a local inverse distance weighted interpolation method.

Sugita et al. (2014) took advantage of line-scanning laser ophthalmoscope (LSLO) for eye motion artifact correction and speckle noise reduction of polarization sensitive optical coherence tomography (PS-OCT). From its first demonstration for measurements in biological samples (Hee et al. (1992)), PS-OCT has become one of the most important tools among the functional extensions of OCT that can assess more than the basic tomographic images of the reflected light intensity (Pircher et al. (2006b), Yamanari et al. (2008), Yasuno et al. (2010)). In their work, the tracking is done by correcting actuations of the PS-OCT horizontal/vertical-scanner according to the offset signals based on the retinal position shifts detected by the LSLO. At first, a template image with a reference marker such as a thick blood vessel branch of the retina is chosen and extracted from the LSLO images. During the data acquisition of the PS-OCT subsystem, the LSLO images are captured in parallel and the the cross-correlation between the template and each LSLO image is computed. Using the cross-correlation values, the best match is found and the horizontal/vertical shifts are obtained. Then a correction signal proportional to the computed shift information is sent to the PS-OCT XY-scanner. Using this system, they were able to achieve tracking rates of up to 60Hz for correcting the involuntary eye motions during PS-OCT data acquisition.

Similar to the work of Capps et al. (2011), Kocaoglu et al. (2014) focus on designing a system for correcting eye motion for AO-OCT. Because of AO-OCT's cellular resolution, it is a more demanding modality for retinal stabilization in comparison to SLO or OCT. In their work, the tracker is integrated in the sample arm of the 2nd generation Indiana AO-OCT system. The core of the Indiana AO-OCT system is a SD-OCT imager, which uses a broadband femtosecond laser (Integral OCT, Femto Lasers, Vienna, Austria) with central wavelength at 800 *nm* and bandwidth of 160 *nm* in its source arm. The detection channel of the SD-OCT system is designed based on a Basler Sprint camera and A-scan rate of 167 KHz is achieved. The tracker consisted of three subsystems: dynamic tracking for retina stabilization, secondary wide field imaging for navigating and monitoring the system operation, and a programmable fixation target for controlling subject's gaze. The tracker portion was designed to stabilize the location of the imaging beam relative to the location of the optic disc. The second subsystem is a wide field line-scan scanning ophthalmoscope that provides a 35° × 35° real-time fundus view. The third was a fixation channel, a LCD display that was integrated into the tracker module for extending the tracker monitor display. To evaluate the performance of the tracker and as the first step of post-processing of the acquired AO-OCT volumes, the axial motions are corrected. This is followed by segmenting the two layers corresponding to inner segment/outer segment junction (IS/OS) and posterior tip of the outer segment (PTOS) of the cone photoreceptors. Finally, using a combination of manual and strip-based software registration the performance of the tracker for AO-OCT imaging is measured and optimized.

3.2. Software-Based Approaches

Having a truthful approximation of the eye motion during OCT data acquisition makes the problem of correction more reliable and robust. This was the case for hardware-based techniques in which, using additional hardware, the patterns of eye motion were determined and later used for correcting the locations of A-scans/B-scans in OCT volume data. For software-based techniques, the procedure of correction needs prior assumptions about the nature of eye motion which is not always satisfied. Therefore the problem is highly non-linear and ill-posed at its very core. Technically speaking, the patterns of eye motion are in three dimensions with possibility of translation and rotation and we observe only non-linear projections of these 3D transformations. Having additional hardware for measuring eye motions during OCT acquisition makes the matter of motion correction almost trivial. This is obvious from the above-mentioned papers in which the utilized motion estimation techniques were all variations of strip-based registration using cross-correlation as metric with minimal differences from paper to paper. In those papers the main focus is on the implementation aspects of building such devices rather than the software used for correcting the acquired data. In contrast, more innovation is needed for creating software algorithms to do the task. Of course it should be mentioned that software based techniques can only achieve an approximation of the eye motion pattern which is very case-specific and limited.

Speckle noise degrades the quality of OCT scans drastically and makes the process of interpretation of the data for image registration very hard. But this can be considered as the easiest problem to solve since other limitations play a bigger role here. Due to the layered anatomy of the retina, most of the B-scans look the same with minimal variations in discriminating features, like blood vessel shadows and also in regions near fovea and optic nerve head (ONH). This adds additional complexity to the problem of motion correction since it makes tracking of specific features in the images very hard. Axial motions due to heartbeat, respiration and head motion can be observed by viewing the data orthogonal to the plane of acquired B-scans. But one should keep in mind that the retina has its own curvature which is hard to be distinguished from the axial artifacts. Using multiple orthogonal volume scans, this problem can be solved for the most part since the individual B-scans have minimal motion artifacts. But transverse motion artifacts still have high impacts on the data. Transverse motion artifacts are caused by eye movement in the 2D plane created by fast and slow scanning axes. When this happens only parallel to the plane of B-scans it is called *in-plane* and can be observed by locating breaks in the prominent features such as blood vessels. The most problematic case happens when the transverse motions happen *out-of-plane*, or in another word, along the slow scanning axis. In this case, depending on the direction of the motion which can be along the positive or negative direction of the axis, it can cause multiple copies of some regions of the retina or can cause gaps in the acquired data. This type of eye motion is almost impossible to quantify. This section contains overviews of several well-known software-based techniques for eye motion artifact reduction in OCT data.

Zawadzki et al. (2007b,a) use ImageJ (Schneider et al. (2012)) for correcting both axial and lateral motion of the OCT volume data. Axial motion correction is done by maximizing 2D cross-correlation between consecutive B-scans. Using this technique, one is able to modify volume data so that the orthogonal view has less axial motion artifacts in comparison to the original data. Of course the true curvature of the retina cannot be restored using this technique. The same technique was used for lateral/transverse motion correction too. But as they mentioned in their works, lateral motion artifacts were minimal in the data so only axial motion correction suffices. They also didn't consider the possibility of *out-of-plane* motion along the slow scanning axis.

Developments of ultra-high speed OCT devices can reduce the problem of eye motion artifacts substantially. In the work of Potsaid et al. (2008) four ultra-high speed OCT system designs based on a CMOS line scan camera (Sprint spL4096-140k from Basler Vision Technologies) are presented and compared. The designs presented differ in several factors including number of pixels used on the camera, light source/spectrum, spectrometer design, ophthalmic imaging module optics, and line rate/exposure time and can achieve acquisition speeds in the ranges of 70,000 to 312,500 A-scans per second. The first configuration shows improved sensitivity roll-off with imaging depth by utilizing a high resolution spectrometer configuration while imaging at a speed of 70,000 A-scans per second. The second, demonstrates higher axial resolution and larger spectrometer pixel count while imaging at over 100,000 A-scans per second. The third configuration images at 250,000 A-scans per second, which is an order of magnitude faster than commercial systems. Finally, the fourth configuration images at 312,500 axial scans per second, which was the fastest reported *in vivo* imaging of the human eye by any OCT method at the time of publication. At these high speeds, transverse motion artifacts are minimal, how-ever, the acquired data still suffer from axial artifacts due to very fine axial resolution. Using the third configuration, they were able to image a volume of $512 \times 512 \times 400$ in 1.3 seconds. For correcting the axial motion artifacts, they used a globally optimized technique rather than relying on maximizing cross-correlations between consecutive B-scans which while performing reasonable locally, cannot preserve the global curvature of the retina. Due to the very high speed, taking few additional B-scans does not requires significant additional scanning time since each B-scan takes about 2.0 milliseconds to be captured. Therefore, right before each horizontal raster scan, three vertical B-scans (one at each edge and one at the center of the volume of interest) are acquired. As one can imagine the eye motion during an individual B-scan is negligible. Therefore, by registering each horizontal B-scan to the three vertical scans, it is possible to eliminate the effects of axial eye motion almost completely. This was done by 3×3 pixel averaging and spatial filtering of axial scans in the horizontal volume scan at the location of intersection with the three vertical B-scans and running an exhaustive search for minimizing the sum of squared differences (SSD) with the 3×1 averaged axial profiles at the same location in the three vertical scans. Using this technique a globally optimized axial correction can be achieved. Figure 6 shows an example of this technique for axial motion correction of an OCT volume data.

In any image registration technique, the transformation is found between two images; one as a reference image which is kept unchanged and one as a moving image (or template) which is deformed assuming some constraints dictating the extent and type of deformation (rigid, non-rigid, deformable etc) (Baghaie and Yu (2014), Baghaie et al. (2014)). Having a reference image of the retina with minimal motion artifacts, it is possible to correct the OCT data. In the work of Ricco et al. (2009) the problem of transverse motion correction has been dealt with by using a SLO image as the reference. Since the SLO frame is captured almost instantaneously, it can be considered artifact free. The method uses blood vessels as means for registering. For detecting blood vessels, a modified version of the method proposed by Lam and Yan (2008) which uses hysteresis thresholding to find ridges in the divergence of the image gradient is adopted. Using 0.2 and 0.075 as upper and lower thresholds, respectively, the blood vessels are detected. This step is followed by removing areas with less than five pixels. For correcting tremors and drift, the elastic image registration technique proposed by Periaswamy and Farid (2003) is used. For correcting micro-saccades, dynamic time warping (Sakoe and Chiba (1978)) is used. Assuming the result of the previous step and the SLO image both as signals in the time domain, this technique tries to find the least cost set of feasible correspondences between the two signals. The cost function is defined based on the squared difference in pixel intensities. At the end, an additional iteration of elastic registration will correct the residual artifacts. Of course, this technique is only useful for transverse motion artifact reduction and not the axial motion correction. However, *out-of-plane* motion cannot be corrected.

In the work of Cense et al. (2009), eye motion artifact correction is not the main focus since the paper is largely about comparison of two ultra-broadband sources (multiplexed superluminescent diodes (SLDs) and femtosecond lasers) that can be used in AO-OCT, namely Femtolasers Integral Ti:Sapphire laser and Superlum BroadLighter T840. Volume images were acquired at 6 degree eccentricity superior and inferior to the foveal center as well as the foveal center. These regions are representative of the main areas of retina containing distinct stratification of the major neural layers, extensive network of retinal capillaries in the plexiform layers, large cone photoreceptors surrounded by rod photoreceptors and also fovea which is of significat clinical interest. As for post-processing, only the volumes that show minimal motion artifacts are chosen. For registering the data, first, the location of the A-scans in each B-scan are slid along the axial direction for maximizing the cross-correlation with their neighbors. This was done recursively with different size of regions of interest until stabilized positions were achieved. This step was followed by registering the whole B-scans to one another again in the axial direction. As mentioned in the article, their attempt for registering the B-scans in transverse directions failed due to not being able to separate alignment signals from speckle noise along these axes. The final result is a flattened volume data in which the natural curvature of the retina is eliminated. Of course this is not always a bad thing and in some application, the true curvature of retina is not important.

In the work of Wojtkowski (2010), extensive details are given regarding the imaging basics and also application of high-speed optical coherence tomography systems. As an example, preliminary results demonstrating applicability of high-speed OCT imaging for in vivo functional optical imaging of the intact retina of animal model have been demonstrated by Srinivasan et al. (2006). In this paper, the volumes are of size $160\mu m \times 160\mu m \times 1200\mu m$ corresponding to $64 \times 64 \times 1024$ pixels, acquired at a rate of 24,000 A-scans per second. Each raster scan takes up to 162 milliseconds (approximately 6.2 volumes per second). After acquiring several raster scans of the same location, the transverse eye motions are corrected by using cross-correlation and cropping of consecutive datasets. By using this technique, they were able to increase the average amplitude reflectance of the photoreceptor outer segments by 10–15%. As one can see, having a grid of 64 $\times$ 64 is very coarse and at the rate of 6.2 volumes per second, the amount of eye motion cannot be very big to begin with. In the work of Kocaoglu et al. (2011), imaging of retinal nerve fiber bundles (RNFBs) using OCT and AO is the main topic. Here, only the axial motion correction is done by shifting B-scans axially to align the connecting cilia reflections of the photoreceptors. Examples of uncorrected transverse motion artifacts can be seen in the composite images they provided in their manuscript.

In the work of Lee et al. (2011), they provided an end-to-end pipeline for OCT data analysis of optic nerve head (ONH) which includes a module for axial motion correction. They used a variation of maximum cross-correlation technique (Hee et al. (1995)) based on the assumption of having minimal motion artifacts with individual B-scans. For each frame the amount of shift needed for maximizing cross-correlation between the current frame and its neighbor computed. As mentioned before, such a technique may compensate the axial motion artifacts; but it also eliminates the natural curvature of the retina. To reduce these distortions, the profile view is fitted to a smooth curve instead of a flat line. The procedure is done in an interactive manner, giving the operator the possibility to vary the cubic-spline parameters in order to get the results as needed.

Use of thin-plate splines (TPS) is being investigated in the work of Antony et al. (2011) for automatic axial motion corrections of SD-OCT volume datasets. In this method, at first, the surface between the inner and outer segments of the photoreceptor cells is segmented using a graph-theoretic approach (Garvin et al. (2009)). This is followed by two stages of curve fitting using smoothing TPSs for detecting distinct motion artifacts in OCT images. The first is for estimation and correction of tilt artifacts which are common in B-scans along the fast scanning axis. The second stage is for fitting the TPSs for modeling and correction of motion artifacts seen in the orthogonal view along the slow scanning direction. Due to having different shapes, different strategies are employed for macular and ONH centered scans with different smoothing parameters and numbers of control points for TPSs. The method provides them with a volume that is flattened. Reconstruction of the true scleral curvature is possible by having orthogonal volume scans of the same location in retina. This technique only deals with axial motions and the final result still contains transverse motion artifacts. Even though the axial and transverse components of motion artifacts can be dealt with separately most of the time, in case of having severe transverse motion artifacts in the orthogonal volume scans, the final curvature may contain errors. Figure 7 shows an example of the algorithm for axial motion correction of an OCT volume data.

Modeling the process of OCT data acquisition as a dynamic time-dependent state-space system is considered in the work of Xu et al. (2012) and a particle filtering approach is introduced for correcting axial and transverse eye motion artifacts. Here the problem is considered as an object tracking problem in the dynamic system and for more stability, axial and transverse motion corrections are dealt with separately. At first, the 3D location of a few equally distant A-scans are considered as the state space. For each state, a set of weighted samples is generated as representative particles from the previous frame. Here, Gaussian and uniform distributions are used for generating the particle sets for each state for transverse and axial motion corrections, respectively. The system dynamics for predicting the object movements is chosen as a linear regressive model and the observation is defined based on a window-based similarity measure (mean of absolute differences) between the state in the previous frame and the current particle set. For modeling the transverse motion artifacts, it is necessary to have axially-independent representations of the A-scans. For this, two different 1-D Haar-function filters with different window sizes are applied on each A-scan and max, min, max-min, and zero to fourth order central moments of the responses are taken as features. Mean, standard deviation, skewness, and kurtosis are also taken from each A-scan. For axial motion modeling, the whole A-scans are considered. Finally, the state posterior distribution is approximated by the observations of weighted particles. The displacement of each given state in current B-scan is obtained by estimating the functional state's expectation. Even though very innovative, the amount of transverse motion artifacts are only considered to be between 2–10 pixels which is very limited. Moreover, the true curvature of the retina is eliminated here since the axial alignment causes the volume to be flattened. Motions along the slow-scanning axis cannot be corrected using this method.

In the work of Hendargo et al. (2013) the main focus is on eye motion correction in speckle variance OCT data of vasculature network. Datasets are $2.5mm \times 2.5mm$ volume scans with 300 A-scans per B-scan, 3 repeated B-scans at each location for computing the variance and 300 unique B-scan locations which adds up to 900 B-scans per each volume scan. Considering multiple volume scans from each subject, half of the scans are oriented along the horizontal axis as the fast scanning axes while the other half are oriented along the vertical axes as the fast scanning axes. The axial motion is corrected by maximizing cross-correlation between consecutive B-scans. Average of the 3 repeated B-scans are computed to improve the signal-to-noise-ratio (SNR) and the variance of the three at each location is computed as the speckle variance data, resulting in 300 variance B-scans. Speckle variance data show higher vessel contrast in comparison to the reflectance data that show higher retinal layer contrast. Therefore the speckle variance data is used to guide the registration algorithm while the reflectance data is used for layer segmentation. Image registration was done on the summed volume projections (SVP) of the ganglion cell plexus since larger vessels are located in this layer and this can improve the performance of image registration. The computed transformation are then directly applied to the SVPs of the superficial (IPL-INL junction) and deep (INL-OPL junction) capillary plexuses. Break locations in the OCT data which correspond to saccades during data acquisition appear as very bright streaks along the fast scanning axis and therefore can be detected and used for dividing the SVPs into saccade-free strips. This is followed by eliminating strips of less than 25 B-scans as they contain little information for proper registration. After vessel contrast enhancement using a set of Gabor filters, the largest strip is chosen as the starting point for registration and the largest strip from the orthogonal scan is registered to it using cross-correlation maximization. To account for small deformable misalignments, a B-spline based deformable registration is employed next. The two registered strips are then averaged and used as reference for registering other strips in the same manner (global rigid registration by cross-correlation maximization and local deformable registration by B-spline based technique). Finally, the computed transformations are applied to the other SVPs. Combining the results of several 3D datasets with at least 50% overlap provides a wide-field mosaic of the blood vessel structure of the retina. Using speckle variance data for detecting breaks, it is possible to account for transverse eye motions along the slow-scanning axis (*out-of-plane*) to some extent. However this cannot be considered as the final and accurate solution to the problem since the amount of gap or overlap introduced to the data in the time of acquisition cannot be measured. An example of the output of the algorithm can be seen in Figure 8.

Kraus et al. published two papers dealing with the problem of involuntary eye motion artifacts during OCT data acquisition (Kraus et al. (2012, 2014)). In both of these techniques several orthogonal OCT volume scans are used for axial and transverse motion correction. The first approach (Kraus et al. (2012)) tries to solve the problem by moving individual A-scans to minimize a global energy functional. In a sense the proposed algorithm is an image registration based technique while there are subtle differences both in formulation and also in the theory behind the method. In general image registration techniques, one image is considered to be as a reference that does not deform while the other image (template) can deform in a way so some metric can be optimized. Here, both the reference and template volumes can deform and two dense displacement fields are computed. The other difference is in the way they regularized their energy minimization functional. Depending on the type of motion that a registration method is intended for (rigid, non-rigid, deformable etc), a regularization term can be defined which puts some constraints on the extent of spatial deformation that can occur. Here, the regularization is not defined on the spatial deformations but instead it is applied to the derivative of the displacements with respect to time. This is based on the assumption of having small displacements between the input volumes. Choosing this regularizer means that the computed displacements may not be smooth spatially. Even though this is probably the case needed here, since we can have sudden breaks and *out-of-plane* motions, the outcome is unpredictable and very dependent on the chosen parameters. After minimizing the energy functional, the distortions are removed and the corrected volumes are merged to create a single volume with higher SNR and lower motion artifacts. For pre-processing, each A-scan is filtered using median filtering in order to reduce the effect of speckle noise and then sub-sampled by a factor of 2 for reducing the computational complexity of the method. The volumes are normalized to have zero mean and unit variance. The energy functional for the registration is defined as:

$$F(Disp(t)) = \sum_{v1=1}^{N_v} \sum_{v2=v1+1}^{N_v} \theta(v1, v2) \|R_{v1,v2}\|^2 + \alpha \int_t \| \left(\frac{\partial Disp(t)}{\partial t}\right)^T \begin{bmatrix} 1 & 0 & 0 \\ 0 & 1 & 0 \\ 0 & 0 & \sqrt{\alpha_z} \end{bmatrix} \|^2 \partial t \quad (1)$$

where F is the objective to be minimized, R is the residuals between volumes, θ is 0 or 1 depending whether a certain pairing of input volumes contributes to the objective function or not and α is the regularizer's weight. The optimization process is done iteratively and in a multi-resolution manner using Gaussian reduction of the volumes. After each iteration, it is required to re-sample the deformed volumes to a regular 3D grid. This is done by employing a cubic Hermite spline method to interpolate the data. For testing their algorithm, they acquired data in a $6 \times 6 mm^2$ area by 400×400 A-scans or $12 \times 12 mm^2$ area by 1100×1100 A-scans using two OCT prototypes with scan rates of 70,000 and 200,000 A-scans per second, respectively. These two fast scanning prototypes provide the ground for having small motion artifacts as it is assumed in the formulation of the method. The paper claims that using the proposed technique, it is possible to estimate the relative motion between the device and the retina. While this claim can be close to the truth in case of having minimal motion artifacts, it is not true in general. Computing the *true* relative motion between the device and the retina means finding the *global minimizer* for the problem of eye motion artifact correction. But since the problem itself is highly non-linear and ill-posed, finding the global solution is impossible to begin with and every algorithm tries to find a better approximation in comparison to the previous ones.

In their later work Kraus et al. (2014) try to introduce some modifications to their previously mentioned method. In the previous method, they used sum of squared differences (SSD) as the metric for defining the difference between the volumes for driving the optimization. Since in SSD, the error contributions from outliers dominate the objective function, this can be problematic, especially in OCT volume registration since the data is highly degraded by speckle noise. To remedy this issue, they have used a modified version of pseudo-Huber loss function which approximates the L_1 norm rather than SSD which measures L_2 norm. This function is defined as:

$$Huber(\mathbf{x}, \varepsilon_H) = \sum_{n=1}^{N} (\varepsilon_H (\sqrt{1 + (\frac{x_n}{\varepsilon_H})^2} - 1)) \qquad (2)$$

where x_n is the nth component of the vector $\mathbf{x}$ and ε_H is set to a small number 0.001. This function approximates L_1 norm for absolute values of x_n significantly bigger than ε_H. The same thing can happen for the regularization term since it is also based on squared loss metric. Using squared loss, individual high gradients are penalized dis-proportionally. Here, the previous regularization term is replaced with an approximation of the $L_{0.5}$ norm defined as:

$$L_{0.5,\varepsilon_{0.5}}(\mathbf{x}) = \sum_{n=1}^{N} (\sqrt{\sqrt{x_n^2 + \varepsilon_{0.5}}} - \sqrt{\sqrt{\varepsilon_{0.5}}}) \qquad (3)$$

where $\varepsilon_{0.5}$ is chosen to be 0.1. This formulation of regularization term can help in having a better compensation of saccades. They use a two stage optimization here, with the first stage being the rough axial correction based on the method they presented in the previous paper and second stage being the full optimization based on the method with modifications mentioned earlier. They have also added tilt correction and mean displacement regularization as well as illumination correction in their algorithm. For acquiring the data, again, a very limited setting is chosen. The volumes are acquired from a $6mm \times 6mm$ area by 200×200 A-scans and managed to reduce the eye motion in the volumes. Figure 9 shows an example of using this algorithm for eye motion artifact reduction of orthogonal OCT volume scans.

One of the very recent examples of software based techniques for eye motion reduction is the work of Montuoro et al. (2014). The proposed method is based on the hypothesis that for the most part, a perfectly motion free SD-OCT volume from a healthy person is *predominantly* locally symmetric along the axial scan direction. This implies that the appearance of a small region is similar in both the fast and slow scanning directions. As accurately mentioned in the paper, even in a perfectly motion free volume scan this is not completely true, especially around the fovea and also in regions with pathology, hence the term "predominantly" in the hypothesis. The main focus of the paper is on axial motion correction based on the local symmetry assumption. For correcting the axial motion, at first, an A-scan is chosen and then a window along the fast and slow scan axes is extracted. Local curvatures along both fast and slow axes are computed and used for finding the amount of needed shift along the axial direction. Given that the A-scan was chosen randomly, it is possible that the local symmetry assumption did not hold for this A-scan. This issue can be reduced by repeating the above steps for multiple A-scans in the same B-scan and averaging the results. The absolute displacement vector can now be calculated by averaging all the computed shifts. For transverse motion correction, after flattening the volume, the familiar phase correlation technique between neighbor B-scans is used. As is obvious from the presented results, the main contribution of the method is in axial motion correction. For the 100 real OCT volumes, only 19 cases were improved transversely, while 14% degraded and the rest stayed the same. It should also be mentioned that axial motion correction with the assumption of local symmetry, may cause pathologies to be flattened. Of course more analysis is needed for better assessing the performance of the method.

4. Discussion

As mentioned before, the reason for categorizing all of the methods for eye motion correction into two classes, namely hardware-based techniques and software-based techniques, is based on the observations made when investigating literature in this area. So even though hardware-based techniques usually use custom software for interpreting the data on the eye motion patterns during OCT acquisition, since the software is not the focus of the paper and also since almost all of the techniques use variations of cross-correlation-based registration with minimal differences, this was not used as a ground for our categorization. Instead, the classification is based on the fact that whether an approach acquires additional information about the eye motion patterns during OCT acquisition by using additional hardware in the system or not.

Tables 2 and 3 provide a complete overview of the hardware and software-based techniques for involuntary eye motion artifact reduction in OCT systems and Table 4 provides an overview of the pros and cons of hardware and software based techniques. The following subsections contain detailed discussion about each class and the approaches taken by the researchers.

For the problem of eye motion artifact reduction in OCT data, being *truthful* means providing a result that doesn't contain any motion artifacts and is *anatomically correct*. This is critical since the experts use such data to make judgment calls about the well-being of a patient. Therefore having an anatomically correct result is the first and most important requirement from any approach. Of course in different cases, this can mean slightly different things. For example if only the *en face* view of a volume scan is needed, then the axial motion artifacts are not important since the *en face* view is generated by summing up all the information along the axial direction. In this case, only transverse motion artifacts are the ones that need to be considered.

4.1. Hardware-Based Approaches: Discussion

Overall, since hardware-based techniques have a direct access to the eye motion patterns during the OCT acquisition time, they are capable of representing anatomically truthful volume scans as outputs. One thing that stands out when reviewing the hardware-based approaches for eye motion artifact reduction is the fact that in all of the cases, axial and transverse motion compensations are treated separately. Not only that, but also it is obvious that the most focus is put to correct transverse motion artifacts using additional hardware and rely on simple software based techniques (cross-correlation maximization, for example) for axial motion correction. Depending on the application, this may be acceptable, but one needs to consider that use of cross-correlation maximization techniques does not guarantee a truthful reconstruction of the curvature of the retina.

In the works of Pircher et al. (2007, 2010) axial motion compensation is done by tracking the apex of cornea which is different than the rest of the papers in the class of hardware-based techniques. Two other papers from the same class use feature tracking as means for motion compensation, but this time for transverse motions. Ferguson et al. (2004) and Kocaoglu et al. (2014) use the lamina cribrosa and optic disk as features for tracking and compensating the transverse motion artifacts in an online manner, respectively. The rest of the papers use some variations of strip-based registration of SLO frames for motion estimation during the OCT acquisition time. The general idea behind strip-based registration of SLO frames is based on the assumption of having minimal motion artifacts during acquisition of several line scans in each frame. Choosing an appropriate SLO frame from the sequence (either a single frame or a composite of several frames) as the reference, the strips are registered and finally the motion is estimated based on the position of the strip within the frame and also the location of the OCT beam at that exact time-point. From the mathematical point of view, such techniques have nothing new to offer since they are mostly based on cross-correlation maximization. But in such techniques, there is no need for very sophisticated image registration approaches since the assumption of having minimal motion artifacts within strips is practically strong.

Another major benefit for using hardware-based techniques when compared with software-based techniques is in the capability of compensating *out-of-plane* motions. As mentioned before, eye motion is a combination of rotations and translations that happen in 3 dimensions and capturing OCT volumes only provides us with projections of such motions in 1 or 2 dimensions. Axial and transverse motion compensations are de-coupled and computed separately even though in a strict sense, such de-coupling will incur some small errors. This is the case for all of the hardware-based techniques. By considering the two components separately, *out-of-plane* motions will be mostly limited to the transverse component of the motion. The interesting thing about hardware-based techniques is that they do not care about the motion and whether it is *in-plane* or *out-of-plane* since they have captured the needed information about the eye motion pattern during acquisition. This means that even though the eye can move in a non-linear manner during the time of data acquisition, since the tracking information (either from feature tracking or SLO frame acquisition) is acquired continuously, a very accurate approximation of the motion can be computed and then compensated in the OCT data.

Hardware-based techniques usually provide a faster solution to the problem of eye motion artifact reduction. This is true even for the offline techniques since the registration of SLO frames using cross-correlation maximization can be implemented with very efficient software and use of optimized Fast Fourier Transform (FFT) libraries. Implementing them in an online manner, by use of FPGA or GPU devices provides additional capabilities in terms of accuracy and reliability. Works of Vienola et al. (2012) and Braaf et al. (2013) are very good examples of this, since the online implementation of the approaches made it possible to correct for blinks and large saccades by re-scanning the affected areas.

On the negative side, the need for having additional hardware mounted onto the OCT devices for being able to capture supplementary information about the eye motion patterns during OCT acquisition can be considered as a drawback of such hardware-based techniques. This is mainly a problem when using commercial devices which are designed in a compact and closed manner and usually do not allow for alterations. This means that such systems should be built from scratch in most cases. Of course as mentioned before, some of the OCT devices already have hardware-based motion artifact reduction components implemented and in a few years, all will have them on-board.

Even though hardware-based techniques are the most reliable and dominating techniques for eye motion artifact correction, their main drawback is with regard to the inapplicability to the legacy data. Different research centers around the world have acquired tens of thousands of volume datasets over the years from patients that need to be processed. In such cases, hardware-based techniques are completely useless; This is why we need software-based techniques, even though the performance is highly dependent on the quality of the data. It should also be mentioned that many of the hardware-based techniques discussed here are only available in research facilities and having commercially available devices with optimized setups requires time.

4.2. Software-Based Approaches: Discussion

Even though the hardware-based techniques provide more promising results, software-based techniques are more preferable when using commercially available OCT devices since minimal alterations of the machines are possible in such cases. However this is not the sole benefit of using software-based techniques over hardware-based techniques. As mentioned before, one of the biggest drawbacks of hardware-based techniques is the inability to be applied to legacy data. This is a very big issue when it comes to longitudinal studies with data acquired by previous generations of OCT devices. Due to high cost of acquiring and maintaining such data, which are usually managed by major research facilities, it is only reasonable to expect to extract as much information as possible from a dataset before putting it aside. But one needs to draw the line somewhere in terms of the expectations out of software-based techniques for the amount/type of motion artifacts that an algorithm can correct. This is mainly because of the simplifying assumptions that are made in such algorithms.

In hardware-based techniques, using additional hardware with the accompanying software, one could extract the pattern of eye motion during OCT acquisition and then use it to correct the OCT data, either online or offline. In software-based techniques, this information is forever lost and therefore some assumptions should be made about the nature of it. Generally speaking, the problem of image matching and correspondence is an ill-posed inverse problem which requires carefully designed constraints in the process of formulation and computing the solution. When it comes to the problem of involuntary eye motion corrections in OCT data, this can become an NP-hard problem with no globally optimized answer. This is usually the scenario in case of having severe eye motions, especially transverse eye motions. Transverse motion artifacts can be divided into two different classes: 1) *in-plane* motions and 2) *out-of-plane* motions. This categorization is only for being able to classify the methods and in reality, both of these motions happen in OCT volume acquisition.

In-plane motions happen when saccadic eye motion occurs along the direction of fast scanning axis, either in positive or negative directions. Such motion cannot be fully recognized and measured by looking at the consecutive B-scans and they are mainly obvious looking at the *en face* view of the volume. In regions that contain prominent features like blood vessels or optic disk etc., these artifacts are represented with clear breaks in the structure of the features. However, automatic detection and correction of these breaks have been a challenge for years. Having a motion free image as reference can make the problem easier. Ricco et al. (2009) used a SLO frame as reference and tried to correct for such motions by use of dynamic time warping (DTW). It is possible to correct for such motions by using the information gathered from the consecutive B-scans using axially-independent features. In Xu et al. (2012) using particle filtering, several axially-independent features are tracked for being able to compensate for *in-plane* eye motions. Kraus et al. (2012, 2014) used a similar technique but with use of multiple orthogonal scans, based on the assumption of not-having coinciding motion artifacts at the same location in the orthogonal scans. However, success in such techniques is always dependent on the extent and severity of eye motion during OCT acquisition.

The problem of motion artifact correction is even harder in cases of having *out-of-plane* motions. In such cases, not only the structure of the features contained in the images are altered due to eye motion, but also we end up with datasets that contain multiple copies of some portions of data or even missing data on some regions of the retina. Even though caused by the same phenomena, the last two cases have different implications. Multiple copies of some portions of data happen when sudden saccadic eye motions occur in the same direction as the slow scanning axis. On the other hand, if the saccadic motions happen in the opposite direction of slow scanning axis, some portion of the retina will not be imaged. Both of these effects can be observed by looking at the distinct features contained in the OCT volume data. In the former, careful locating of the breaks is the key for correction, although both detection and correction steps are approximations at best. In the later, even if one is able to find the location of the saccade in the OCT data, correction is impossible due to having missing data. A brief investigation of the techniques discussed here is a clear indication of such problems as in almost all of the techniques, none can account for out-of-plane motions. The work by Hendargo et al. (2013) is the only one that can handle these motions mainly because use of speckle variance OCT provides an easy solution to the problem of break detection in OCT volume data. By using the exact location of the breaks caused by saccadic eye motions and taking advantage of multiple orthogonal OCT scans, they are able to account and correct for *out-of-plane* eye motions. It should be noted that comparing consecutive B-scans does not provide a good representation for saccades and *en face* views are mostly used for capturing the effects of such motions. This is why use of cross-correlation based techniques such as the ones presented in (Zawadzki et al. (2007b,a), Cense et al. (2009), Srinivasan et al. (2006)) cannot provide satisfactory results in more corrupted datasets.

Another aspect of being truthful to the actual anatomy of the retina, as discussed previously, is in regards to the ability to reconstruct the true curvature of the retina after motion correction. Like before, cross-correlation maximization based techniques which work based on aligning consecutive B-scans in an OCT volume scan cannot preserve the true curvature of the retina. Assuming use of high-speed OCT imaging devices which are commonplace nowadays, individual B-scans can be considered as axially artifact free. Considering this, true curvature of the retina can be reconstructed simply by acquiring additional orthogonal scans (B-scans or volumes) at the same location of the regular raster scans. This technique and its variations are used in the works of Kraus et al. (2012, 2014), Potsaid et al. (2008), Antony et al. (2011). In Kraus et al. (2012, 2014) having multiple orthogonal scans is the main assumption for optimizing the global energy functional defined for image registration. In Potsaid et al. (2008), only 3 orthogonal B-scans are acquired and used for axial motion correction of the regular raster scanned OCT volume. Antony et al. (2011) put the main focus on axial motion correction in their work and produce a flattened OCT volume as the output which obviously lacks the true curvature of the retina. However given additional orthogonal scans, they are able to reconstruct the true curvature. Of course it should be noted that several premises should be satisfied in order to be able to reconstruct the true curvature of the retina by using additional orthogonal scans: 1) The orthogonal scans should be exactly from the same location as the regular raster scan. 2) Even though considered axially artifact free, B-scans still can contain tilting and illumination artifacts that may complicate the procedure. 3) Sever transverse motion artifacts, *in-plane* and *out-of-plane*, can cause errors in the reconstructed curvature since they are present in both regular raster-scanned and orthogonal volume data.

All of the above mentioned issues encountered in software-based eye motion correction techniques will require the extent of eye motions to be kept at a minimal level during data acquisition. This means that we should have more careful imaging sessions, with higher speed OCT machines in a wider field-of-view using coarser imaging grids. This is mainly the case for transverse motion correction techniques since axial motion artifacts are easier to correct for, especially when having multiple orthogonal scans. Of course it should be noted that even though having OCT imaging devices with higher speeds will definitely improve the process of image acquisition and interpretation of the data since the amount of motion artifacts will be reduced, this comes at the cost of losing sensitivity of the imaging devices which can be problematic, especially in case of subjects with visual diseases like choroideremia, glaucoma, AMD etc. In such cases, fixational eye motions are more common and have a significant effect on the quality of acquired data. This reduces the applicability of software-based techniques drastically. On the other hand, hardware-based techniques, because of their ability to capture information about the eye motion patterns in the time of data acquisition, can perform more reliably and accurately for reconstructing anatomically accurate 3D representation of the *in vivo* human retina.

5. Conclusion

In the current work, a comprehensive review of the state-of-the-art in involuntary eye motion correction of optical coherence tomography data is provided. Starting from general remarks regarding the importance of OCT in current clinical settings, a general overview is given regarding several different aspects of OCT image analysis, including: noise reduction, feature segmentation and image registration. For each class, several different techniques are mentioned briefly with proper references for further reading. As for the application of image registration techniques in OCT data analysis, examples in noise reduction, multi-modal registration, image mosaicing and eye motion corrections are given. Since the focus in this paper is on the latter, eye motion reduction, at first the general problem is discussed in great detail and factors causing eye motion artifacts are introduced. After categorizing the state-of-the-art technique into two major classes, namely hardware-based and software-based techniques, several examples of each class are introduced and discussed in detail. Additional discussions are provided in regard to the advantages and disadvantages of hardware/software-based techniques. Overall, hardware-based techniques are shown to have better performance in comparison to software-based techniques. At the same time, longitudinal studies can benefit immensely from development of new software-based approaches to make use of the vast amount of OCT data available in research centers.

Acknowledgments

The authors would like to thank Dr. Joseph Carroll from Advanced Ocular Imaging Program (AOIP), Medical College of Wisconsin (MCW) for providing the data and insight. This work was partially supported by NIH P30EY001931. Support received by grant 8UL1TR000055 from the Clinical and Translational Science Award (CTSA) program of the National Center for Research Resources and the National Center for Advancing Translational Sciences. Support received by the Clinical & Translational Science Institute of Southeast Wisconsin through the Advancing a Healthier Wisconsin endowment of the Medical College of Wisconsin.

The authors would also like to express their sincere gratitude to the anonymous reviewers for their invaluable comments and suggestions for improving the work.

References

Adler DC, Ko TH, Fujimoto JG. Speckle reduction in optical coherence tomography images by use of a spatially adaptive wavelet filter. Optics letters. 2004; 29(24):2878–2880. [PubMed: 15645810]

Alonso-Caneiro D, Read SA, Collins MJ. Speckle reduction in optical coherence tomography imaging by affine-motion image registration. Journal of biomedical optics. 2011; 16(11):116027–1160275. [PubMed: 22112132]

Antony B, Abramoff MD, Tang L, Ramdas WD, Vingerling JR, Jansonius NM, Lee K, Kwon YH, Sonka M, Garvin MK. Automated 3-d method for the correction of axial artifacts in spectral-domain optical coherence tomography images. Biomedical optics express. 2011; 2(8):2403–2416. [PubMed: 21833377]

Avanaki MR, Cernat R, Tadrous PJ, Tatla T, Podoleanu AG, Hojjatoleslami SA. Spatial compounding algorithm for speckle reduction of dynamic focus oct images. Photonics Technology Letters, IEEE. 2013; 25(15):1439–1442.

Baghaie, A., D'souza, RM., Yu, Z. Sparse and low rank decomposition based batch image alignment for speckle reduction of retinal oct images. Biomedical Imaging (ISBI), 2015 IEEE 12th International Symposium on; IEEE; 2015a. p. 226-230.

Baghaie A, D'souza RM, Yu Z. Application of independent component analysis techniques in speckle noise reduction of retinal oct images. Optik-International Journal for Light and Electron Optics. 2016; 127(15):5783–5791.

Baghaie, A., Yu, Z. Computational Modeling of Objects Presented in Images. Fundamentals, Methods, and Applications. Springer; 2014. Curvature-based registration for slice interpolation of medical images; p. 69-80.

Baghaie A, Yu Z, D'souza RM. State-of-the-art in retinal optical coherence tomography image analysis. Quantitative Imaging in Medicine and Surgery. 2015b; 5(4):603–617. [PubMed: 26435924]

Baghaie, A., Yu, Z., Dsouza, RM. Advances in Visual Computing. Springer; 2014. Fast mesh-based medical image registration; p. 1-10.

Barlow HB. Eye movements during fixation. The Journal of Physiology. 1952; 116(3):290–306. [PubMed: 14939180]

Braaf B, Vermeer KA, Sicam VAD, van Zeeburg E, van Meurs JC, de Boer JF. Phase-stabilized optical frequency domain imaging at 1-μm for the measurement of blood flow in the human choroid. Optics express. 2011; 19(21):20886–20903. [PubMed: 21997098]

Braaf B, Vermeer KA, Vienola KV, de Boer JF. Angiography of the retina and the choroid with phase-resolved oct using interval-optimized backstitched b-scans. Optics express. 2012; 20(18):20516–20534. [PubMed: 23037099]

Braaf B, Vienola KV, Sheehy CK, Yang Q, Vermeer KA, Tiruveedhula P, Arathorn DW, Roorda A, de Boer JF. Real-time eye motion correction in phase-resolved oct angiography with tracking slo. Biomedical optics express. 2013; 4(1):51–65. [PubMed: 23304647]

Canon-Europa-N.V. [Accessed: 11-10-2016] Oct-hs100. Http://www.canon.co.uk/medical/eyecare/oct-hs100/

Capps, AG., Zawadzki, RJ., Yang, Q., Arathorn, DW., Vogel, CR., Hamann, B., Werner, JS. SPIE BiOS. International Society for Optics and Photonics; 2011. Correction of eye-motion artifacts in ao-oct data sets; p. 78850D-78850D.

Carl-Zeiss-Meditec. [Accessed: 11-10-2016] Cirrus hd-oct. Http://www.zeiss.com/meditec/enus/products-solutions/ophthalmology-optometry/glaucoma/diagnostics/optical-coherence-thomography/oct-optical-coherence-tomography/cirrus-hd-oct.html

Carpenter, RH. Movements of the eyes. Pion Limited; 1988. 2nd rev

Cense B, Koperda E, Brown JM, Kocaoglu OP, Gao W, Jonnal RS, Miller DT. Volumetric retinal imaging with ultrahigh-resolution spectral-domain optical coherence tomography and adaptive optics using two broadband light sources. Optics express. 2009; 17(5):4095–4111. [PubMed: 19259249]

Chiu SJ, Izatt JA, OConnell RV, Winter KP, Toth CA, Farsiu S. Validated automatic segmentation of amd pathology including drusen and geographic atrophy in sd-oct images. Invest Ophthalmol Vis Sci. 2012; 53(1):53–61. [PubMed: 22039246]

Chiu SJ, Li XT, Nicholas P, Toth CA, Izatt JA, Farsiu S. Automatic segmentation of seven retinal layers in sdoct images congruent with expert manual segmentation. Optics express. 2010; 18(18):19413–19428. [PubMed: 20940837]

de Kinkelder R, Kalkman J, Faber DJ, Schraa O, Kok PH, Verbraak FD, van Leeuwen TG. Heartbeat-induced axial motion artifacts in optical coherence tomography measurements of the retina. Investigative ophthalmology & visual science. 2011; 52(6):3908–3913. [PubMed: 21467182]

DeBuc, DC. A review of algorithms for segmentation of retinal image data using optical coherence tomography. INTECH Open Access Publisher; 2011.

Drexler W, Fujimoto JG. State-of-the-art retinal optical coherence tomography. Progress in retinal and eye research. 2008; 27(1):45–88. [PubMed: 18036865]

Estrada R, Tomasi C, Cabrera MT, Wallace DK, Freedman SF, Farsiu S. Enhanced video indirect ophthalmoscopy (vio) via robust mosaicing. Biomedical optics express. 2011; 2(10):2871–2887. [PubMed: 22091442]

Fang L, Li S, McNabb RP, Nie Q, Kuo AN, Toth C, Izatt J, Farsiu S, et al. Fast acquisition and reconstruction of optical coherence tomography images via sparse representation. Medical Imaging, IEEE Transactions on. 2013; 32(11):2034–2049.

Fang L, Li S, Nie Q, Izatt JA, Toth CA, Farsiu S. Sparsity based denoising of spectral domain optical coherence tomography images. Biomedical optics express. 2012; 3(5):927–942. [PubMed: 22567586]

Fercher AF. Optical coherence tomography. Journal of Biomedical Optics. 1996; 1(2):157–173. [PubMed: 23014682]

Fercher AF, Drexler W, Hitzenberger CK, Lasser T. Optical coherence tomography-principles and applications. Reports on progress in physics. 2003; 66(2):239.

Ferguson RD, Hammer DX, Paunescu LA, Beaton S, Schuman JS. Tracking optical coherence tomography. Optics letters. 2004; 29(18):2139–2141. [PubMed: 15460882]

Fernández DC, Villate N, Puliafito C, Rosenfeld P. Comparing total macular volume changes measured by optical coherence tomography with retinal lesion volume estimated by active contours. Investigative Ophthalmology & Visual Science. 2004; 45(13):3072–3072.

Garvin MK, Abràmoff MD, Kardon R, Russell SR, Wu X, Sonka M. Intraretinal layer segmentation of macular optical coherence tomography images using optimal 3-d graph search. Medical Imaging, IEEE Transactions on. 2008; 27(10):1495–1505.

Garvin MK, Abràmoff MD, Wu X, Russell SR, Burns TL, Sonka M. Automated 3-d intraretinal layer segmentation of macular spectral-domain optical coherence tomography images. Medical Imaging, IEEE Transactions on. 2009; 28(9):1436–1447.

Golabbakhsh M, Rabbani H. Vessel-based registration of fundus and optical coherence tomography projection images of retina using a quadratic registration model. IET Image Processing. 2013; 7(8):768–776.

Guo Q, Dong F, Sun S, Lei B, Gao BZ. Image denoising algorithm based on contourlet transform for optical coherence tomography heart tube image. Image Processing, IET. 2013; 7(5):442–450.

Gupta D, Anand R, Tyagi B. Ripplet domain non-linear filtering for speckle reduction in ultrasound medical images. Biomedical Signal Processing and Control. 2014; 10:79–91.

Hee MR, Izatt JA, Swanson EA, Huang D, Schuman JS, Lin CP, Puliafito CA, Fujimoto JG. Optical coherence tomography of the human retina. Archives of ophthalmology. 1995; 113(3):325–332. [PubMed: 7887846]

Hee MR, Swanson EA, Fujimoto JG, Huang D. Polarization-sensitive low-coherence reflectometer for birefringence characterization and ranging. JOSA B. 1992; 9(6):903–908.

Heidelberg-Engineering. [Accessed: 11-10-2016] Spectralis hra-oct. http://www.heidelbergengineering.com/us/products/spectralis-models/

Hendargo HC, Estrada R, Chiu SJ, Tomasi C, Farsiu S, Izatt JA. Automated non-rigid registration and mosaicing for robust imaging of distinct retinal capillary beds using speckle variance optical coherence tomography. Biomedical optics express. 2013; 4(6):803–821. [PubMed: 23761845]

Huang D, Swanson EA, Lin CP, Schuman JS, Stinson WG, Chang W, Hee MR, Flotte T, Gregory K, Puliafito CA, et al. Optical coherence tomography. Science. 1991; 254(5035):1178–1181. [PubMed: 1957169]

Jian Z, Yu L, Rao B, Tromberg BJ, Chen Z. Three-dimensional speckle suppression in optical coherence tomography based on the curvelet transform. Optics express. 2010; 18(2):1024–1032. [PubMed: 20173923]

Jian Z, Yu Z, Yu L, Rao B, Chen Z, Tromberg BJ. Speckle attenuation in optical coherence tomography by curvelet shrinkage. Optics letters. 2009; 34(10):1516–1518. [PubMed: 19448806]

Jørgensen TM, Thomadsen J, Christensen U, Soliman W, Sander B. Enhancing the signal-to-noise ratio in ophthalmic optical coherence tomography by image registration method and clinical examples. Journal of biomedical optics. 2007; 12(4):041208–041208. [PubMed: 17867797]

Kafieh R, Rabbani H, Abramoff MD, Sonka M. Intra-retinal layer segmentation of 3d optical coherence tomography using coarse grained diffusion map. Medical image analysis. 2013a; 17(8): 907–928. [PubMed: 23837966]

Kafieh R, Rabbani H, Kermani S. A review of algorithms for segmentation of optical coherence tomography from retina. Journal of medical signals and sensors. 2013b; 3(1):45. [PubMed: 24083137]

Kobayashi M, Hanafusa H, Takada K, Noda J. Polarization-independent inter-ferometric optical-time-domain reflectometer. Lightwave Technology, Journal of. 1991; 9(5):623–628.

Kocaoglu OP, Cense B, Jonnal RS, Wang Q, Lee S, Gao W, Miller DT. Imaging retinal nerve fiber bundles using optical coherence tomography with adaptive optics. Vision research. 2011; 51(16): 1835–1844. [PubMed: 21722662]

Kocaoglu OP, Ferguson RD, Jonnal RS, Liu Z, Wang Q, Hammer DX, Miller DT. Adaptive optics optical coherence tomography with dynamic retinal tracking. Biomedical optics express. 2014; 5(7):2262–2284. [PubMed: 25071963]

Kraus MF, Liu JJ, Schottenhamml J, Chen CL, Budai A, Branchini L, Ko T, Ishikawa H, Wollstein G, Schuman J, et al. Quantitative 3d-oct motion correction with tilt and illumination correction, robust similarity measure and regularization. Biomedical optics express. 2014; 5(8):2591–2613. [PubMed: 25136488]

Kraus MF, Potsaid B, Mayer MA, Bock R, Baumann B, Liu JJ, Hornegger J, Fujimoto JG. Motion correction in optical coherence tomography volumes on a per a-scan basis using orthogonal scan patterns. Biomedical optics express. 2012; 3(6):1182–1199. [PubMed: 22741067]

Lam BSY, Yan H. A novel vessel segmentation algorithm for pathological retina images based on the divergence of vector fields. Medical Imaging, IEEE Transactions on. 2008; 27(2):237–246.

LaRocca F, Dhalla AH, Kelly MP, Farsiu S, Izatt JA. Optimization of confocal scanning laser ophthalmoscope design. Journal of biomedical optics. 2013a; 18(7):076015–076015. [PubMed: 23864013]

LaRocca F, Nankivil D, Farsiu S, Izatt JA. Handheld simultaneous scanning laser ophthalmoscopy and optical coherence tomography system. Biomedical optics express. 2013b; 4(11):2307–2321. [PubMed: 24298396]

Lee S, Young M, Sarunic MV, Beg MF. End-to-end pipeline for spectral domain optical coherence tomography and morphometric analysis of human optic nerve head. Journal of Medical and Biological Engineering. 2011; 31(2):111–119.

Li Y, Gregori G, Knighton RW, Lujan BJ, Rosenfeld PJ. Registration of oct fundus images with color fundus photographs based on blood vessel ridges. Optics express. 2011a; 19(1):7–16. [PubMed: 21263537]

Li Y, Gregori G, Lam BL, Rosenfeld PJ. Automatic montage of sd-oct data sets. Optics express. 2011b; 19(27):26239–26248. [PubMed: 22274209]

Lurie KL, Angst R, Ellerbee AK. Automated mosaicing of feature-poor optical coherence tomography volumes with an integrated white light imaging system. Biomedical Engineering, IEEE Transactions on. 2014; 61(7):2141–2153.

Makita S, Hong Y, Yamanari M, Yatagai T, Yasuno Y. Optical coherence angiography. Optics Express. 2006; 14(17):7821–7840. [PubMed: 19529151]

Martinez-Conde S, Macknik SL, Hubel DH. The role of fixational eye movements in visual perception. Nature Reviews Neuroscience. 2004; 5(3):229–240. [PubMed: 14976522]

Mishra A, Wong A, Bizheva K, Clausi DA. Intra-retinal layer segmentation in optical coherence tomography images. Optics express. 2009; 17(26):23719–23728. [PubMed: 20052083]

Montuoro, A., Wu, J., Waldstein, S., Gerendas, B., Langs, G., Simader, C., Schmidt-Erfurth, U. Medical Image Computing and Computer-Assisted Intervention–MICCAI 2014. Springer; 2014. Motion artefact correction in retinal optical coherence tomography using local symmetry; p. 130-137.

Nachmias J. Two-dimensional motion of the retinal image during monocular fixation. JOSA. 1959; 49(9):901–907.

Novotny HR, Alvis DL. A method of photographing fluorescence in circulating blood in the human retina. Circulation. 1961; 24(1):82–86. [PubMed: 13729802]

Optovue-Inc. [Accessed: 11-10-2016] Rtvue. Http://www.optovue.com/products/rtvue/

Periaswamy S, Farid H. Elastic registration in the presence of intensity variations. Medical Imaging, IEEE Transactions on. 2003; 22(7):865–874.

Physical-Sciences-Inc. [Accessed: 11-10-2016] Cirrus hd-oct. Http://www.psicorp.com/products/laser-based-sensors/compact-adaptive-optics-retinal-imager-caori

Pircher M, Baumann B, Götzinger E, Hitzenberger CK. Retinal cone mosaic imaged with transverse scanning optical coherence tomography. Optics letters. 2006a; 31(12):1821–1823. [PubMed: 16729082]

Pircher M, Baumann B, Sattmann H, Hitzenberger CK, et al. Simultaneous slo/oct imaging of the human retina with axial eye motion correction. Optics express. 2007; 15(25):16922–16932. [PubMed: 19550983]

Pircher M, Go E, Leitgeb R, Fercher AF, Hitzenberger CK, et al. Speckle reduction in optical coherence tomography by frequency compounding. Journal of Biomedical Optics. 2003; 8(3):565–569. [PubMed: 12880365]

Pircher M, Gotzinger E, Findl O, Michels S, Geitzenauer W, Leydolt C, Schmidt-Erfurth U, Hitzenberger CK. Human macula investigated in vivo with polarization-sensitive optical coherence tomography. Investigative Ophthalmology and Visual Science. 2006b; 47(12):5487. [PubMed: 17122140]

Pircher M, Götzinger E, Sattmann H, Leitgeb RA, Hitzenberger CK. In vivo investigation of human cone photoreceptors with slo/oct in combination with 3d motion correction on a cellular level. Optics express. 2010; 18(13):13935–13944. [PubMed: 20588526]

Pizurica A, Jovanov L, Huysmans B, Zlokolica V, De Keyser P, Dhaenens F, Philips W. Multiresolution denoising for optical coherence tomography: a review and evaluation. Current Medical Imaging Reviews. 2008; 4(4):270–284.

Potsaid B, Gorczynska I, Srinivasan VJ, Chen Y, Jiang J, Cable A, Fujimoto JG. Ultrahigh speed spectral/fourier domain oct ophthalmic imaging at 70,000 to 312,500 axial scans per second. Optics express. 2008; 16(19):15149–15169. [PubMed: 18795054]

Puvanathasan P, Bizheva K. Interval type-ii fuzzy anisotropic diffusion algorithm for speckle noise reduction in optical coherence tomography images. Optics express. 2009; 17(2):733–746. [PubMed: 19158887]

Ricco, S., Chen, M., Ishikawa, H., Wollstein, G., Schuman, J. Medical Image Computing and Computer-Assisted Intervention–MICCAI 2009. Springer; 2009. Correcting motion artifacts in retinal spectral domain optical coherence tomography via image registration; p. 100-107.

Riggs LA, Ratliff F, Cornsweet JC, Cornsweet TN. The disappearance of steadily fixated visual test objects. JOSA. 1953; 43(6):495–500.

Sakoe H, Chiba S. Dynamic programming algorithm optimization for spoken word recognition. Acoustics, Speech and Signal Processing, IEEE Transactions on. 1978; 26(1):43–49.

Salinas HM, Fernández DC. Comparison of pde-based nonlinear diffusion approaches for image enhancement and denoising in optical coherence tomography. Medical Imaging, IEEE Transactions on. 2007; 26(6):761–771.

Schmitt J. Array detection for speckle reduction in optical coherence microscopy. Physics in Medicine and Biology. 1997; 42(7):1427. [PubMed: 9253050]

Schmitt JM, Xiang S, Yung KM. Speckle in optical coherence tomography. Journal of biomedical optics. 1999; 4(1):95–105. [PubMed: 23015175]

Schneider CA, Rasband WS, Eliceiri KW, et al. Nih image to imagej: 25 years of image analysis. Nat methods. 2012; 9(7):671–675. [PubMed: 22930834]

Sheehy CK, Yang Q, Arathorn DW, Tiruveedhula P, de Boer JF, Roorda A. High-speed, image-based eye tracking with a scanning laser ophthalmoscope. Biomedical optics express. 2012; 3(10):2611–2622. [PubMed: 23082300]

Srinivasan PP, Heflin SJ, Izatt JA, Arshavsky VY, Farsiu S. Automatic segmentation of up to ten layer boundaries in sd-oct images of the mouse retina with and without missing layers due to pathology. Biomedical optics express. 2014; 5(2):348–365. [PubMed: 24575332]

Srinivasan V, Wojtkowski M, Fujimoto J, Duker J. In vivo measurement of retinal physiology with high-speed ultrahigh-resolution optical coherence tomography. Optics letters. 2006; 31(15):2308–2310. [PubMed: 16832468]

Sugita M, Zotter S, Pircher M, Makihira T, Saito K, Tomatsu N, Sato M, Roberts P, Schmidt-Erfurth U, Hitzenberger CK. Motion artifact and speckle noise reduction in polarization sensitive optical coherence tomography by retinal tracking. Biomedical optics express. 2014; 5(1):106–122.

Tao YK, Farsiu S, Izatt JA. Interlaced spectrally encoded confocal scanning laser ophthalmoscopy and spectral domain optical coherence tomography. Biomedical optics express. 2010; 1(2):431–440. [PubMed: 21258478]

Tomlins PH, Wang R. Theory, developments and applications of optical coherence tomography. Journal of Physics D: Applied Physics. 2005; 38(15):2519.

Vienola KV, Braaf B, Sheehy CK, Yang Q, Tiruveedhula P, Arathorn DW, de Boer JF, Roorda A. Real-time eye motion compensation for oct imaging with tracking slo. Biomedical optics express. 2012; 3(11):2950–2963. [PubMed: 23162731]

Wojtkowski M. High-speed optical coherence tomography: basics and applications. Applied Optics. 2010; 49(16):D30–D61. [PubMed: 20517358]

Xu J, Ishikawa H, Wollstein G, Kagemann L, Schuman JS. Alignment of 3-d optical coherence tomography scans to correct eye movement using a particle filtering. Medical Imaging, IEEE Transactions on. 2012; 31(7):1337–1345.

Xu J, Ou H, Lam EY, Chui P, Wong KK. Speckle reduction of retinal optical coherence tomography based on contourlet shrinkage. Optics letters. 2013; 38(15):2900–2903. [PubMed: 23903174]

Yamanari M, Makita S, Yasuno Y. Polarization-sensitive swept-source optical coherence tomography with continuous source polarization modulation. Optics Express. 2008; 16(8):5892–5906. [PubMed: 18542701]

Yannuzzi LA, Slakter JS, Sorenson JA, Guyer DR, Orlock DA. Digital indocyanine green videoangiography and choroidal neovascularization. Retina. 1992; 12(3):191–223. [PubMed: 1384094]

Yarbus, AL. Eye movements during perception of complex objects. Springer; 1967.

Yasuno Y, Yamanari M, Kawana K, Miura M, Fukuda S, Makita S, Sakai S, Oshika T. Visibility of trabecular meshwork by standard and polarization-sensitive optical coherence tomography. Journal of biomedical optics. 2010; 15(6):061705–061705. [PubMed: 21198153]

Yazdanpanah A, Hamarneh G, Smith BR, Sarunic MV. Segmentation of intra-retinal layers from optical coherence tomography images using an active contour approach. Medical Imaging, IEEE Transactions on. 2011; 30(2):484–496.

Zawadzki RJ, Capps AG, Kim DY, Panorgias A, Stevenson SB, Hamann B, Werner JS. Progress on developing adaptive optics–optical coherence tomography for in vivo retinal imaging: Monitoring and correction of eye motion artifacts. Selected Topics in Quantum Electronics, IEEE Journal of. 2014; 20(2):322–333.

Zawadzki RJ, Choi SS, Jones SM, Oliver SS, Werner JS. Adaptive optics-optical coherence tomography: optimizing visualization of microscopic retinal structures in three dimensions. JOSA A. 2007a; 24(5):1373–1383. [PubMed: 17429483]

Zawadzki, RJ., Fuller, AR., Choi, SS., Wiley, DF., Hamann, B., Werner, JS. Biomedical Optics (BiOS) 2007. International Society for Optics and Photonics; 2007b. Correction of motion artifacts and scanning beam distortions in 3d ophthalmic optical coherence tomography imaging; p. 642607-642607.

Highlights

- A brief overview is given about different aspects of retinal Optical Coherence Tomography (OCT) image analysis.
- The problem of involuntary eye motion artifacts during OCT acquisition is described in details.
- A comprehensive literature review of the hardware/software based techniques for eye motion artifact reduction is provided.
- Detailed discussions regarding the effectiveness of the covered methods and directions for future research in this field are presented.

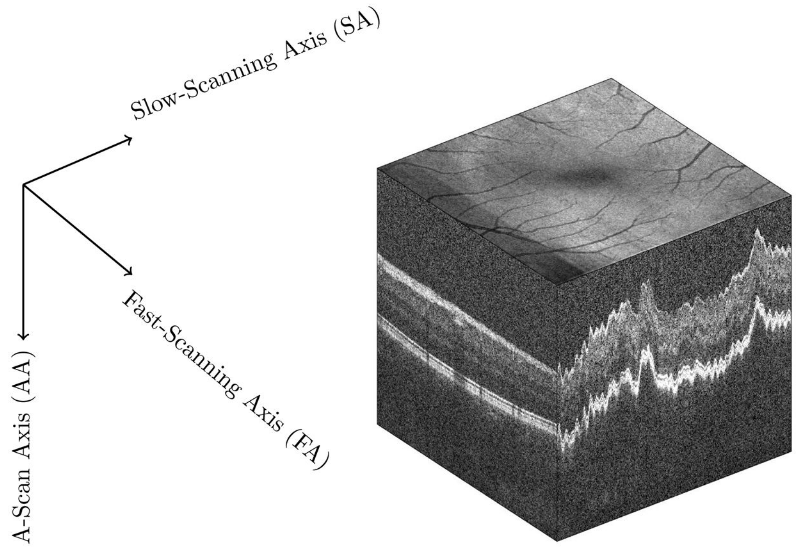

Figure 1.
Sample OCT volume with the corresponding A-scan axis (AA), fast-scanning axis (FA) and slow-scanning axis (SA)

Author Manuscript

Author Manuscript

Author Manuscript

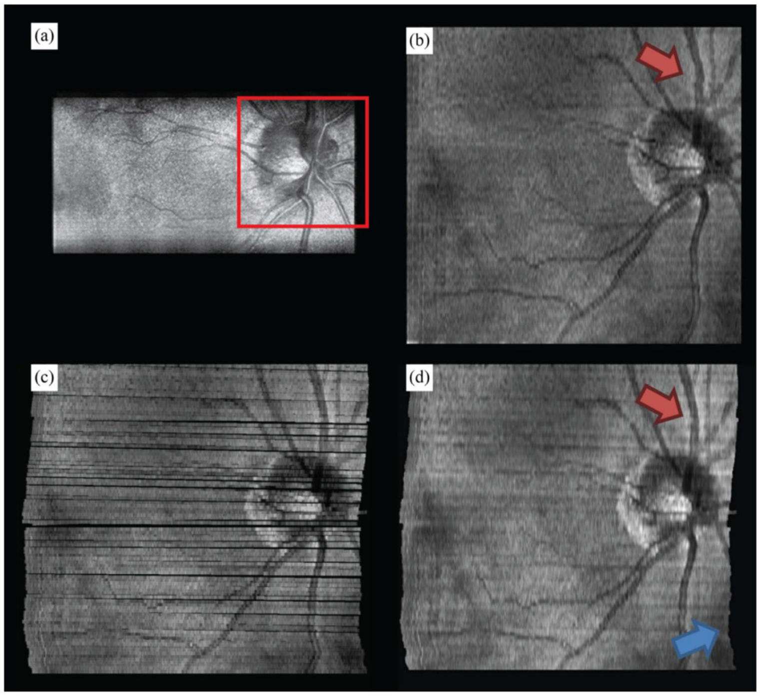

Figure 2.

An example of the work by Tao et al. (2010) for hardware-based eye motion correction using interlaced SECSLO-SDOCT. (a) A region of interest in the SECSLO frame, (b) *en face* view of the SD-OCT volume without correction, (c) *en face* view of the SD-OCT volume after correction, (d) corrected *en face* view re-sampled to a regular image grid. [Reprinted with permission]

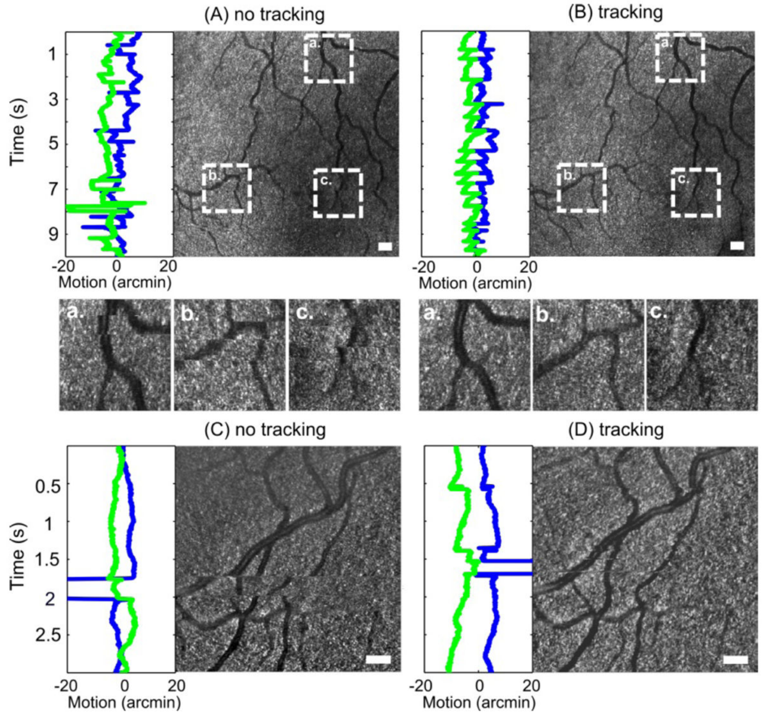

Figure 3.

An example of the work by Vienola et al. (2012) for online motion compensation: (A) and (C) without tracking and (B) and (D) with tracking. The online implementation enables correction of large saccades and re-scanning of the corrupted regions (D). [Reprinted with permission]

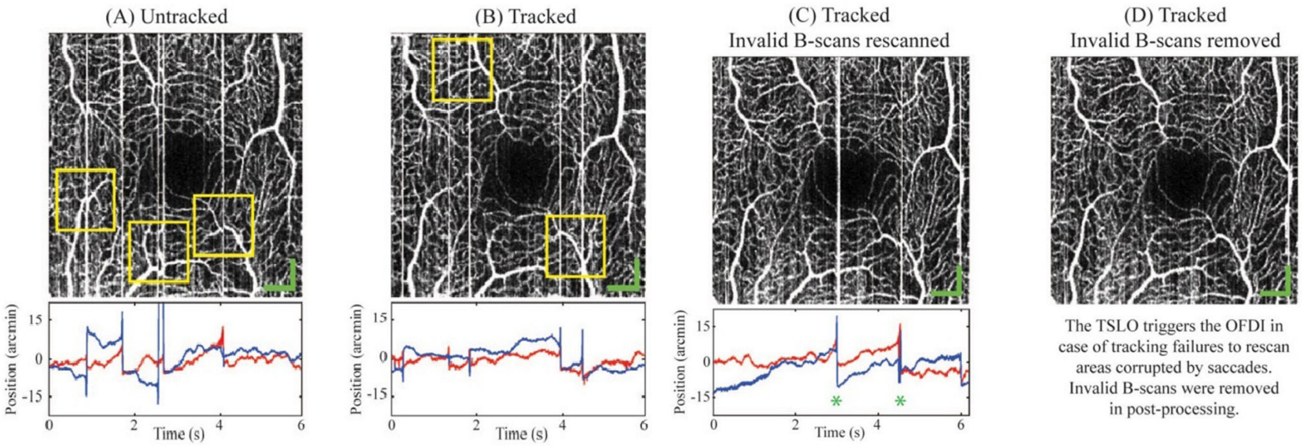

Figure 4.

An examples of eye motion artifacts in phase-resolved OCT angiography of the retina in the work of Braaf et al. (2013). The online implementation enables correction of large saccades and re-scanning of the corrupted regions (D). [Reprinted with permission]

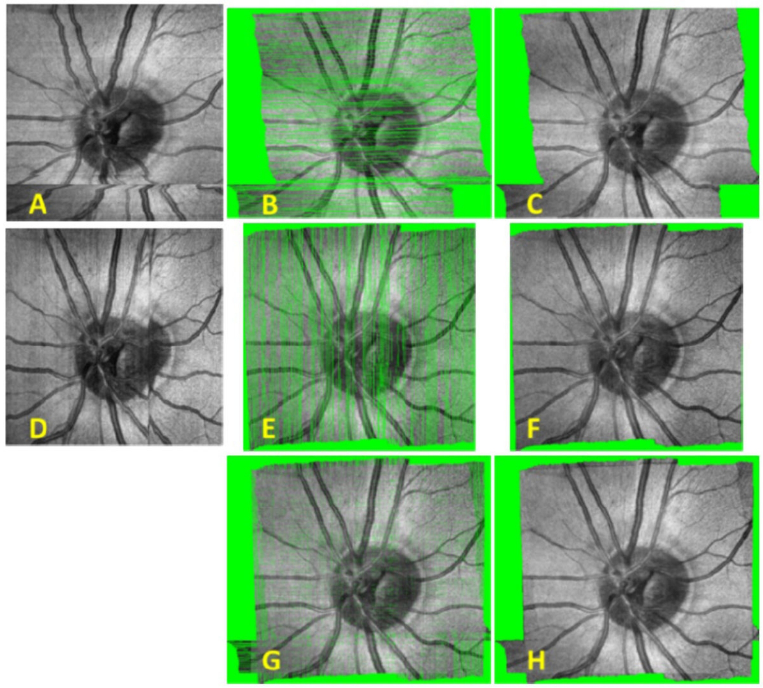

Figure 5.

An example of the work by LaRocca et al. (2013b). The left column shows the two *en face* view of orthogonal scans without motion correction. The middle row displays the SLO-based motion corrected *en face* views without resampling. The right column contains the results of the motion correction after resampling. The images in the bottom row are the results of combining the two *en face* views. [Reprinted with permission]

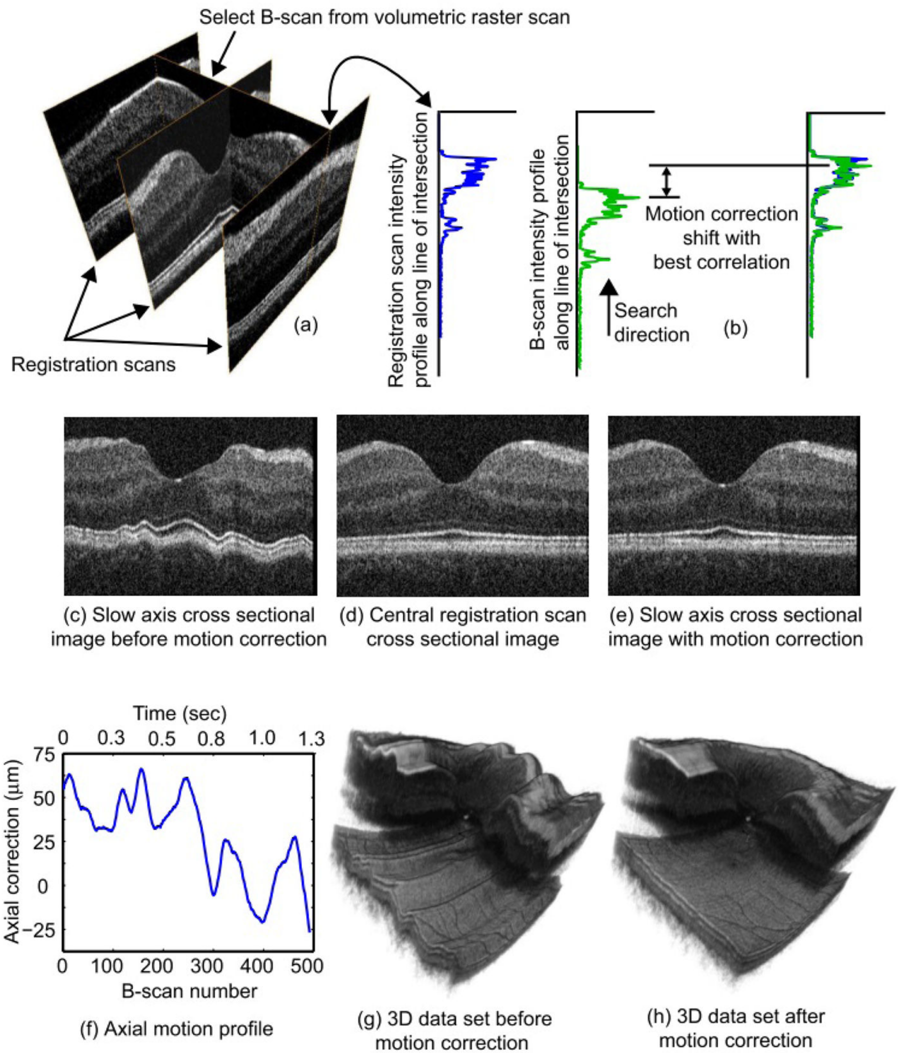

Figure 6.

Axial motion correction by use of three orthogonal B-scans located at the beginning, middle and at the end of the imaged volume (Potsaid et al. (2008)). Using ultra-high speed OCT devices, the true curvature of the retina can be reconstructed with higher degrees of reliability. [Reprinted with permission]

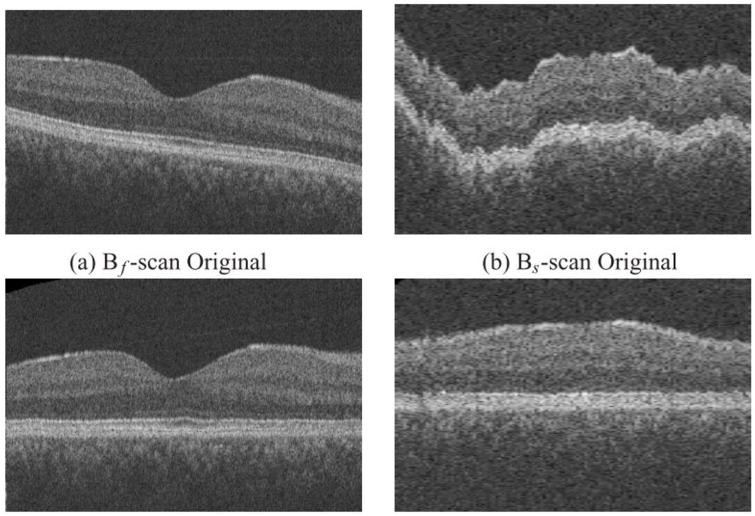

(a) B_f-scan Original (b) B_s-scan Original

(c) B_f-scan Corrected (d) B_s-scan Corrected

Figure 7.

An example of the result of the work by Antony et al. (2011) for axial motion correction of OCT volume scans. *f* and *s* subscripts represent the fast-scanning and slow-scanning axes, respectively. The technique will result in a flattened volume. But with use of orthogonal volume scans, the true curvature of the retina can be reconstructed. [Reprinted with permission]

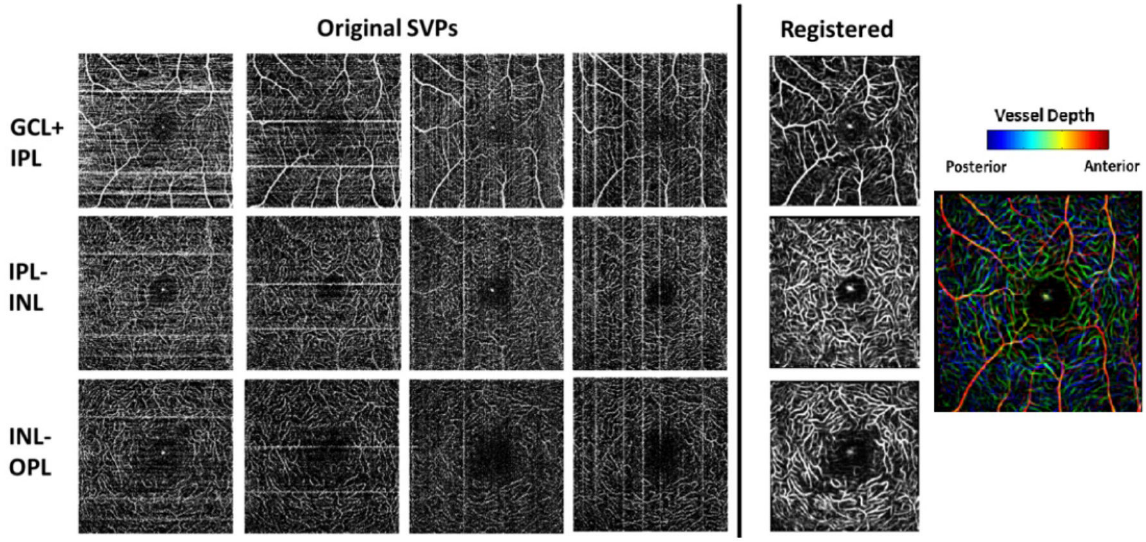

Figure 8.

An example of the work by Hendargo et al. (2013). Two X-fast and two Y-fast datasets were acquired. The original SVPs for each of the three main vessel layers are shown in the left four columns. The fifth column shows the results of image registration for each of the three layers. Each image covers a 2.5 2.5 mm scan area. Motion artifacts are removed and visualization of the vasculature is enhanced in the registered images. A color encoded depth image is shown on the right, combining information from the registered images of the three vessel layers. Red indicates more superficial vessels while blue indicates deeper vessels. [Reprinted with permission]

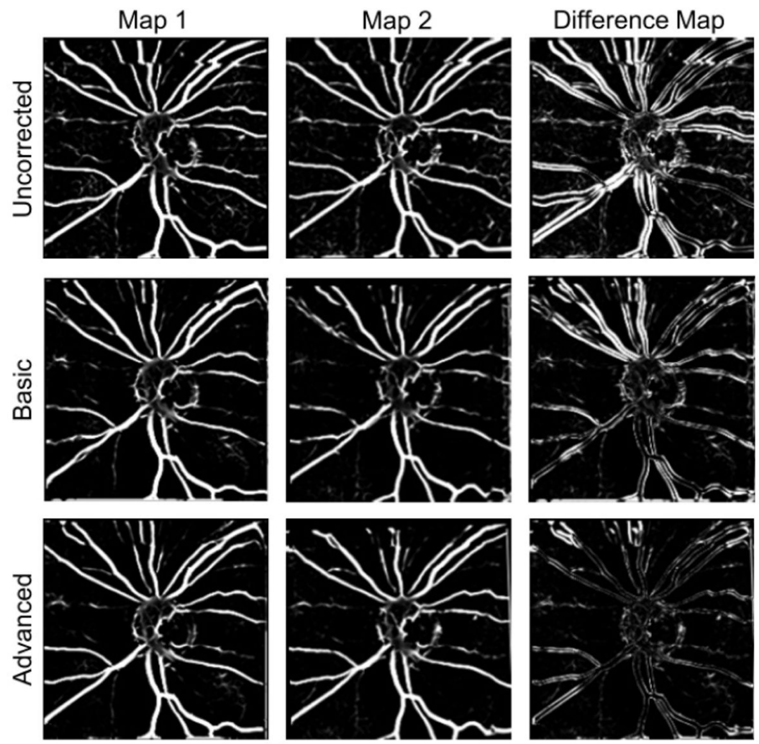

Figure 9.

An example of the work by Kraus et al. (2014). The first row represents the uncorrected blood vessel maps from the two input orthogonal volume scans as well as their difference map. The second row is the result of applying the first stage of the algorithm. The third row is the result of the final stage of the proposed algorithm. [Reprinted with permission]

Table 1

Overview of the methods for correcting involuntary eye motions during OCT data acquisition

Hardware-based	•	Additional hardware for acquiring data on the eye motion patterns;
	•	On-line or off-line;
	•	Axial, transverse & both;
	•	A-scan or B-scan movement for correction, based on the estimated eye motions;
	•	Correcting for blinks or large saccades in on-line regime.
Software-based	•	Assumptions about the eye motion patterns and estimating the motion;
	•	With or without references;
	•	Off-line;
	•	Axial, transverse & both;
	•	A-scan or B-scan movement for correction, based on the estimated eye motions;

Table 2

Overview of the hardware-based methods

Method	Primary Imaging	Secondary Imaging	Features	Axial Correction	Transverse Correction	Blinks
Ferguson et al. (2004)	T-OCT	-	lamina cribrosa	-	online	-
Pircher et al. (2007)	TS-OCT	SD-PCI	cornea	online	-	-
Pircher et al. (2010)	TS-OCT	SD-LCI + RSOD +SLO	cornea	online	offline	-
Tao et al. (2010)	SD-OCT	SEC-SLO	-	-	offline	-
Capps et al. (2011)	AO-OCT	AO-SLO	-	offline (CC-max)	offline	-
Vienola et al. (2012)	OFDI	T-SLO	-	-	online	✓
Braaf et al. (2013)	OFDI	T-SLO	-	offline max) (CC-	online	✓
LaRocca et al. (2013b)	SD-OCT	SLO	-	offline (segmentation based registration)	offline	-
Zawadzki et al. (2014)	AO-OCT	AO-SLO	-	offline (CC-max)	offline	-
Sugita et al. (2014)	PS-OCT	LSLO	-	-	online	-
Kocaoglu et al. (2014)	AO-OCT	LSO	optic disk	-	online (with tracker)	-

T (Tracking), TS (Transversal Scanning), SD-PCI (Spectral Domain Partial Coherence Interferometer), SD-LCI (Spectral Domain Low Coherence Interferometer), RSOD (Rapid Scanning Optical Delay-line), SD (Spectral Domain), SEC-SLO (Spectrally Encoded Confocal Scanning Laser Ophthalmoscope), AO (Adaptive Optics), OFDI (Optical Frequency Domain Imaging), PS (Polarization Sensitive), LSLO (Line-Scanning Laser Ophthalmoscope), LSO (Line-Scan Scanning Ophthalmoscope), CC-max (cross-correlation maximization).

Table 3

Overview of the software-based methods

Method	Device	Scan Area (mm^2)	# of B-scans (line/B-scan)	Speed (A-scans/s)	Axial	Transverse	True Curvature	*out-of-plane*
Zawadzki et al. (2007b)	FD-OCT	-	1001000 200(500)	18,000	CC-max	CC-max	✗	✗
Zawadzki et al. (2007a)	AO-OCT	1 × 1 .25 × .4	1001000 400(250)	18,000	CC-max	CC-max	✗	✗
Potsaid et al. (2008)	FD-OCT	3.9×2.1	512(512)	250,000	SSD-min with additional orthogonal scans	✗	✓	✗
Ricco et al. (2009)	SD-OCT	-	200(200)	-	✗	several steps of registration with a reference SLO frame	✗	✗
Cense et al. (2009)	AO-OCT	.9 × .9	1001000	22,500	CC-max	✗	✗	✗
Srinivasan et al. (2006)	FD-OCT	.16×.16	64(64)	24,000	✗	CC-max	✗	✗
Lee et al. (2011)	SD-OCT	2 × 2	200(800)	19,200	CC-max and manual	✗	~	✗
Antony et al. (2011)	SD-OCT	6 × 6	512(128) 200(200)	18,000 27,000	TPS fitting	✗	✓ (requires additional orthogonal scans)	✗
Xu et al. (2012)	SD-OCT	6 × 6	200(200)	27,000	particle filtering	particle filtering	✗	✗
Hendargo et al. (2013)	SV-OCT	2.5×2.5	300(300)	100,000	CC-max	several steps of strip-based rigid/deformable registration	✗	✓
Kraus et al. (2012)	SD-OCT SS-OCT	6 × 6 12 × 12	400(400) 1100(1100)	70,000 200,000	volume registration with use of additional orthogonal scans	volume registration with use of additional orthogonal scans	✓	✗
Kraus et al. (2014)	SD-OCT	6 × 6	200(200)	26,000	volume registration with use of additional orthogonal scans	volume registration with use of additional orthogonal scans	✓	✗
Montuoro et al. (2014)	SD-OCT	6 × 6	200(200)	18,000 27,000	local curvature compensation	PC-max	✗	✗

FD-OCT (Fourier Domain Optical Coherence Tomography), AO-OCT (Adaptive Optics Optical Coherence Tomography), SD-OCT (Spectral Domain Optical Coherence Tomography), SS-OCT (Swept Source Optical Coherence Tomography), SSD-min (sum of squared difference minimization), CC-max (cross correlation maximization), PC-max (phase correlation maximization), TPS (thin-plate splines)

Table 4

Advantages, disadvantages and limitations of the methods for involuntary eye motion corrections

Hardware-based	Pros	• Can provide *anatomically accurate* volume scans; • Usually faster than software-based techniques; • Can correct for blinks and large saccades (on-line regime);
	Cons	• Needs additional hardware; • Cannot be applied to legacy data; • Hardware implementations need to be customized for the specific application;
Software-based	Pros	• No additional hardware is needed; • Can be applied to legacy data;
	Cons	• The problem is NP-hard, so it needs simplifying assumptions; • It requires very careful image acquisition to eensure minimal motion artifacts; • Usually more time consuming than hardware-based techniques, with moderate success;